Czech Technical University in Prague
Faculty of Electrical Engineering

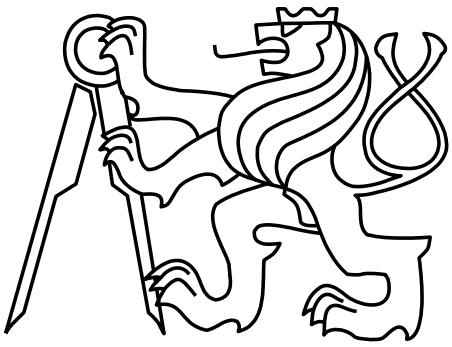

Master's Thesis

Flight Control System for Statically Unstable Small Gliders

Vojtěch Kubica

Thesis supervisor: doc. Ing. Martin Hromčík PhD.

Major: Cybernetics and Robotics
Specialization: Air and Space Systems
May 2018

Prohlášení

Prohlašuji, že jsem předloženou práci vypracoval samostatně a že jsem uvedl veškeré použité informační zdroje v souladu s Metodickým pokynem o dodržování etických principů při přípravě vysokoškolských závěrečných prací.

V Praze, dne 25. května 2018 …….

Podpis

Acknowledgements

First, I would like to express my gratitude to the supervisor doc. Ing. Martin Hromčík Ph.D. for giving me the opportunity to research a topic which has been really close to my heart since my childhood and also for his excellent guidance, caring and patience in answering countless questions. Furthermore, I would like to extend my gratitude to Ing. Pavel Hospodář and Ing. Petr Kočárník, Ph.D., whose advice were also essential to this work. Last, but not least, I would like to thank my family, who kindly offered their help in reviewing this thesis and unconditionally supported me along the way.

Abstrakt

Klouzavý let umožňuje dopravu bez pomoci pohonné jednotky či redukovat potřebu motorového letu. Vylepšení vlastností v kluzu má tedy přímý vliv na spotřebu paliva při plnění cílů jako je například doprava. Současné kluzáky a dopravní letadla, která vlastností v kluzu využívají, létají ve staticky stabilních konfiguracích z důvodu ovladatelnosti člověkem. S dostupností řídících systémů je možné využít i konfigurace, které by za manuálního řízení nedovolovaly bezpečný let. Cílem této studie je prozkoumat možnost zvýšení výkonnosti letadel v klouzavém letu za snížené zásoby stability. Výzkum možnosti vylepšení výkonnosti v klouzavém letu při snížené zásobě stability byl doposud realizován zpravidla bez jasných závěrů. Doporučení v této studii jsou podpořena výsledky simulací a uskutečněnými experimenty na speciálně navrženém modulárním letovém demonstrátoru. Tento prostředek je zkonstruován a je vytvořen jeho matematický model v programu MATLAB Simulink. Různá stabilizační řešení jsou popsána v přehledu existujících řešení, některá jsou implementována prostředí MATLAB Simulink. Vybraná řešení pak stabilizují testovací platformu. Na matematickém modelu jsou demonstrovány změny letových vlastností v závislosti na konfiguraci a míře stability letounu. Poznatky ze simulací jsou použity pro návrh letových testů, které jsou realizovány. Porovnáním reálných testů s výsledky simulací vznikne diskuze možností klouzavého letu za snížené zásoby stability a doporučení pro zlepšení výkonnosti letadel v kluzu.

Klíčová slova: Bezpilotní letadlo, letová výkonnost, klouzavý let, snížená zásoba stability, stabilizace nestabilního letounu.

Abstract

Gliding flight enables an aircraft to fly without a need of a propulsion or reduces the propulsion required. Improvements in glide characteristics have a direct positive effect on fuel consumption. To establish good handling characteristics for a human pilot, current aircraft that utilize the gliding characteristics fly statically stable. With the introduction of modern controllers, an aircraft can fly statically unstable while causing no extra hazard. The goal of this study is to investigate a possibility of flight performance improvement in gliding for an aircraft with relaxed static stability. Previous research on this topic was not very extensive and did not provide clear conclusions. In this work, the determination of possibilities is supported by data from simulations and measurements from real-life flight tests. A custom testbed aircraft was designed and implemented to an accurate mathematical model in MATLAB Simulink. Existing aircraft stabilization solutions were investigated, set in MATLAB Simulink, and the most suitable conformation integrated in the testbed aircraft. Simulations provided conclusions which were used to design the flight-test scenarios. Flight tests were carried out and compared to the simulation results giving differences that result in the possibility of setting recommendations for a gliding flight, particularly with a configuration of relaxed static stability.

Keywords: Unmanned aerial vehicle, flight performance, gliding flight, relaxed static stability, unstable aircraft stabilization.

MASTER‘S THESIS ASSIGNMENT

I. Personal and study details

Student's name: **Kubica Vojtěch** Personal ID number: **406335**

Faculty / Institute: **Faculty of Electrical Engineering**

Department / Institute: **Department of Measurement**

Study program: **Cybernetics and Robotics**

Branch of study: **Air and Space Systems**

II. Master’s thesis details

Master’s thesis title in English:

Flight Control System for Statically Unstable Small Gliders

Master’s thesis title in Czech:

Systém řízení letu pro staticky nestabilní malý kluzák

Guidelines:

The goal of the thesis is to design, verify and experimentally validate control laws for stabilization of flight of a small RC glider. The motivation for this project is expected improvement of performance indicators, namely the range, as compared to a related stable configuration.
1. Develop a simulation model fpr longitudinal dynamics. Implement realistic sensors' models for inertial and aerometric data. Validate the model for selected configurations (stable, marginally stable, unstable).
2. Perform literature survey on existing stabilization approaches for inherently unstable aircraft.
3. Implement and validate selected control laws for flight stabilization in MATLAB Simulink. Consider various variants of sensoric sets.
4. Design and realize a dedicated experimental setup - configurable small RC glider. Mechanical design, servos, control and measurement unit.
5. Experimentally validate selected results and assess the benefits of inhherently unstable configuration with respect to flighjt performance indicators.

Bibliography / sources:

[1] Blakelock: Automatic Control of Aircraft and Missiles, Wiley, 1991, ISBN-10: 0471506516.

Name and workplace of master’s thesis supervisor:

doc. Ing. Martin Hromčík, Ph.D., Department of Control Engineering, FEE

Name and workplace of second master’s thesis supervisor or consultant:

Date of master’s thesis assignment: **26.09.2017** Deadline for master's thesis submission: **25.05.2018**

Assignment valid until: **28.02.2019**

doc. Ing. Martin Hromčík, Ph.D. Supervisor's signature	Head of department's signature	prof. Ing. Pavel Ripka, CSc. Dean's signature

III. Assignment receipt

The student acknowledges that the master's thesis is an individual work. The student must produce his thesis without the assistance of others, with the exception of provided consultations. Within the master's thesis, the author must state the names of consultants and include a list of references.

Date of assignment receipt	Student's signature
.	

TABLE OF CONTENTS

LIST OF FIGURES

LIST OF TABLES

NOMENCLATURE

Acronyms

AHRS	Attitude Heading Reference System
AoA	Angle of Attack
CoG	Center of Gravity
GNSS	Global Navigation Satellite System
GPS	Global Positioning system
IMU	Inertial Measurement Unit
L/D ratio	Lift to Drag ratio
MAC	Mean Aerodynamic Chord
MSL	Mean Sea Level
NP	Neutral Point
RC	Radio Controlled
VLM	Vortex Lattice Method
PWM	Pulse-Width Modulation

Roman symbols

a	Acceleration	$[m/s^2]$
ail_{comm}	Output command for aileron	$[\mu s]$
ail_{diff}	Output for aileron differentiation	$[\mu s]$
$ail_{neutral}$	Output for aileron at neutral position	$[\mu s]$
AR	Aspect ratio	$[-]$
$\bar{c}$	Mean aerodynamic chord	$[m]$
$C_{D_{\alpha^2}}, C_{L_{\alpha^2}}, C_{m_{\alpha^2}}$	Drag, lift, and moment coefficients AoA square derivatives	$[rad^{-2}]$
$C_{D_0}, C_{L_0}, C_{m_0}$	Steady state drag, lift, and moment coefficients	$[-]$
$C_{D_\alpha}, C_{L_\alpha}, C_{m_\alpha}$	Drag, lift, and moment coefficients AoA derivatives	$[rad^{-1}]$
C_{L_Q}, C_{m_Q}	Lift and moment coefficients pitch rate derivatives	$[rad^{-1}]$
$C_{L_{\delta e}}, C_{m_{\delta e}}$	Drag, lift, and moment coefficients AoA square derivatives	$[rad^{-1}]$
C_D	Drag coefficient	$[-]$
C_L	Lift coefficient	$[-]$
C_m	Pitching moment coefficient	$[-]$

C_x	Coefficient with respect to x_{body} axis	$[-]$
C_z	Coefficient with respect to z_{body} axis	$[-]$
e	Oswald factor	$[-]$
$elev_{comm}$	Output command for elevator	$[\mu s]$
$elev_{neutral}$	Output for elevator at neutral position	$[\mu s]$
F	Force	$[N]$
g	Gravitational acceleration	$[m/s^2]$
I_y	Moment of inertia along lateral axis	$[kg \cdot m^2]$
K_d	Gain of differential part	$[\mu s \cdot s/rad]$
K_i	Gain of integral part	$[\mu s/rad]$
K_p	Gain of proportional part	$[\mu s/rad]$
K_u	Ultimate gain	$[\mu s/rad]$
m	Weight	$[kg]$
M	Pitching moment	$[N \cdot m]$
$\bar{q}$	Dynamic pressure	$[pa]$
Q	Pitch rate	$[rad/s]$
R	Pitch rate	$[rad/s]$
R_{body}^{ned}	Transformation matrix from body to NED coordinate system	$[-]$
S	Reference area (main wing)	$[m^2]$
T_u	Ultimate period	$[s]$
T_x	Thrust	$[N]$
U	Longitudinal velocity	$[m/s]$
v	Airspeed	$[m/s]$
W	Vertical velocity	$[m/s]$
X	Longitudinal force	$[N]$
X_e	x-coordinate in Earth coordinate system	$[m]$
Z	Vertical force	$[N]$
Z_e	z-coordinate in Earth coordinate system	$[m]$

Greek symbols

α	Angle of Attack	$[rad]$
γ	Glide angle	$[deg]$
δe	Elevator deflection	$[rad]$
θ	Pitch attitude	$[rad]$
ρ	Air density	$[kg/m^3]$
ϕ	Roll attitude	$[rad]$

Subscripts

$aero$	Aerodynamical
$b, body$	In body coordinate system
$comm$	Command
e	In Earth coordinate system
g	Gravitational
$stab$	In stability coordinate system
tot	Total sum
$trim$	Trimmed

1 INTRODUCTION AND MOTIVATION

The motivation to investigate the flight control systems for small gliders has roots in the author's participation in Radio Controlled (RC) gliders competitions. In these competitions, it is always desired to have a glider with sufficient aerial performance to complete the general competition goal. The performance limits of the competing gliders have been pushed to the maximum by manufacturers specialized on competition glider design. As the performance is highly dependent on pilot skills, pilots started to compensate the disadvantages of visual control. Gyroscopes started to be deployed to establish straight flight path from distances where the visual approach is inefficient. Aircraft performance augmentation, however, can go much further. Particularly, longitudinal static instability could make the glider utilize the advantages like maneuverability at slow speeds close to the ground. Nevertheless, the overall gliding capabilities of the aircraft might get improved as well.

In competition, besides piloting skills, every competitor is trying to gain an advantage over the others by buying even aerodynamically cleaner and lighter glider. This solution leads to a composite aircraft, which is always pricey. Different approach to the flight qualities augmentation presents a challenge and the motivation for investigation of possibilities of improvement.

The goal of this thesis is to investigate relaxed static stability of an aircraft and its effect on flying performance. Among these, rate of sink, L/D ratio, and maneuverability is considered. The set of these flight performance parameters should be an output of various simulations in MATLAB Simulink. To verify the simulations, flight tests on a testbed aircraft should be performed. These flight tests should be designed carefully with respect to aspects that might degrade the aerial verification results and confirm or disprove the classic theory as well as the proposed improvements. Contribution of this thesis is twofold. Firstly, existing conventional approaches will be investigated and verified. Secondly, the flight performance of a statically unstable aircraft has been widely tested only for maneuverability, but not so much for the gliding capabilities. As a conclusion of these thesis, a potential improvement of a configuration with a relaxed static stability will be discussed.

To understand the basics, flight performance and the general background of the thesis is introduced in chapter 2. This report also bases on flight tests with accurate simulations and the testbed aircraft is described in chapter 3. Part of the aircraft design is also the electronic equipment integrating sensoric sets and all this is introduced together with data processing. In this part, some basic

methodology of this thesis is presented. After the aircraft introduction, aircraft dynamics laws and modelling is discussed in chapter **4** together with the creation of mathematical model of the introduced testbed aircraft. In the end of this chapter, aircraft stability of the model is analyzed. chapter **5** describes existing and implemented stabilization and control systems. Firstly, overview of existing solutions is presented. Before the chosen controller design for the testbed aircraft, several solutions are simulated in MATLAB Simulink and discussed. This chapter is concluded with the chosen controllers and their tuning. chapter **6** is dedicated to the first investigation of aerial performance improvement possibilities. Performance improvement is discussed together with the effect of different aerodynamic configuration of an aircraft. chapter **7** is dedicated to aerial tests. In this chapter, tests on the testbed aircraft will be carried out and results of simulations will be verified afterwards. Finally, this master's thesis is concluded and results discussed in chapter **8**.

2 BACKGROUND

2.1 LONGITUDINAL STATIC STABILITY

Longitudinal static stability of an aircraft describes the ability of the aircraft to recover from a non-steady flight caused by a pulse change of the forces that act on it. With positive static stability, a deflection from the steady flight is compensated by the moment of lift forces with respect to the center of gravity. Negative stability causes the aircraft deflecting even more than the initial deflection was and will not recover unless an additional force is applied. Neutral stability is a special case. It means the aircraft has no tendency to deflect from the changed pitch orientation and therefore it will not return to the steady flight it was deflected from.

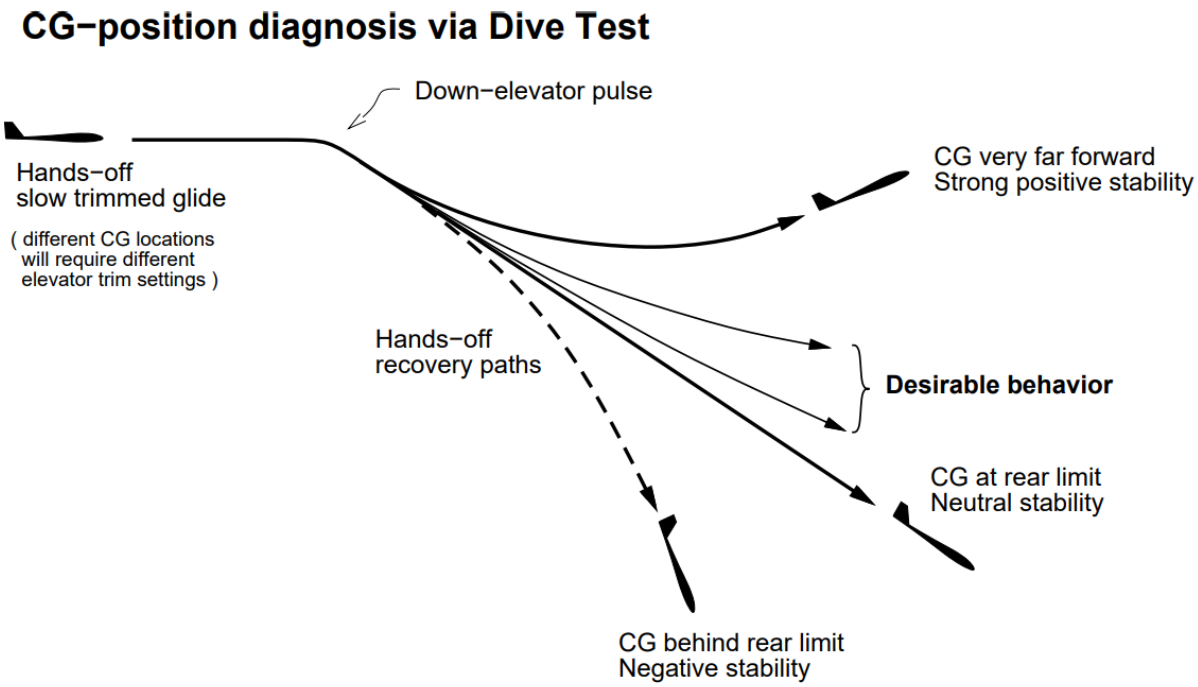

Figure 1: Dive Test and Aircraft Response on Vertical Velocity Gradient (adopted from [1])

To investigate the longitudinal static stability of an aircraft, Dr. Drela presented "Dive Test" [1] visualized in FIGURE 1. "Dive Test" is a method of setting up center of gravity location with respect to the desirable behavior. It is stated that the CoG location has only minor effect on the maximal L/D ratio that means a huge change of the CoG causes only small change of the L/D ratio. This statement is investigated later in this thesis.

According to FIGURE 2, a pilot who controls a glider remotely can benefit from lower stability margin, which causes the airplane to pitch up more when entering a thermal lift and therefore the indication of even smaller lift is significant.

Considering jet fighters, static instability was desired to establish controllability during a supersonic flight, where the aerodynamic center of the wing moves from 25% of mean aerodynamic chord (MAC) to approximately 50% of MAC. This brought a whole new level of maneuverability of the aircraft since the pitch changes were made even without any deflection of the elevator. This way, the aircraft could complete a maneuver with minor action of the control surfaces [2]. However, to be controllable by a human, these aircraft must be loaded with excessive number of computers to secure safety of the system in case of a failure of one unit.

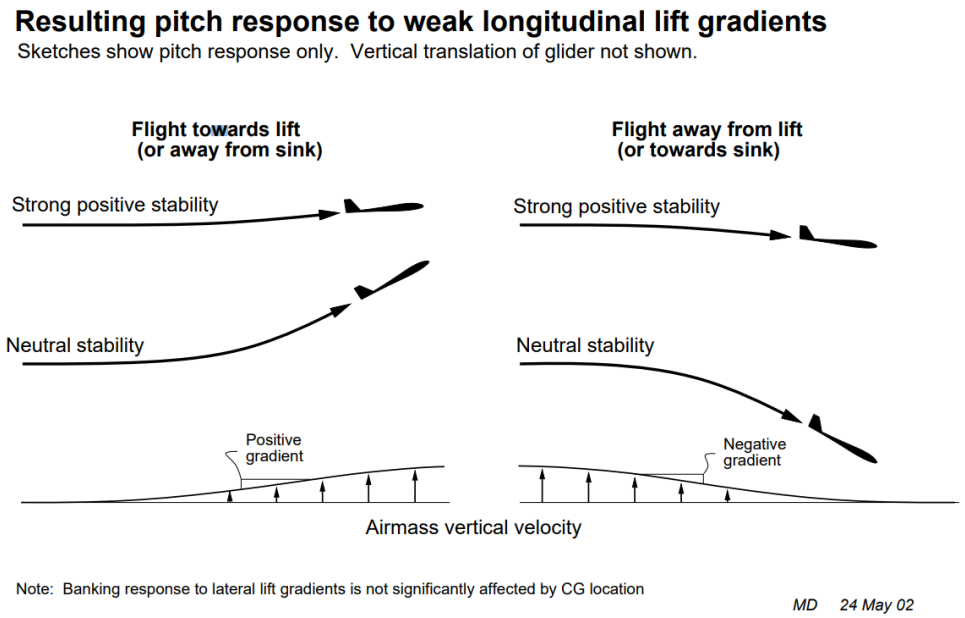

Figure 2: Pitch Response to Weak Longitudinal Lift Gradients (adopted from [1])

2.2 FLIGHT PERFORMANCE

Flight performance of the gliders can be divided into two categories: Pilot-based and aircraft-based performance. The first mentioned is crucial when performing human-controlled flight maneuvers, the other one, however, is significant during every moment of the mid-phase of the flight.

As the glider is also an airplane that weights more than air, without a propulsion unit, it would simply sink to the ground. However, using thermals might significantly extend time in the air as well as the total distance travelled. At smaller altitudes, the thermal diameter is often significantly

smaller than the aircraft's "flat turn" and in this situation, pilot needs to balance the aircraft at the speed not far from stall to be able to circle in this thermal. To maintain the highest gain from the thermal, it is desirable to circle around the thermal center. Additionally, when entering the thermal, it is not known where the thermal center is and therefore must be discovered as soon as possible. These are the examples of pilot influence on the overall flight performance of a glider. It is also noteworthy that the demanded pilot requirements increase when the glider is controlled remotely. As the biggest challenge, a pilot controlling the aircraft from the ground without any telemetry data can be presented. Pilot qualities and their effect is not discussed in this thesis.

Since the aircraft-based qualities of an aircraft are measurable and quantifiable, the investigation of them drags more attention of research. FIGURE 3 shows a typical gliding flight. The main elements of glider performance are the glide ratio, often also referred as lift-to-drag ratio or L/D ratio, and the rate of sink. Glide ratio represents a distance aircraft can fly from unit altitude in the airmass [3]. Flying at the maximum glide ratio brings advantages in a cruise flight to complete distance-based goals. Angle γ is known as a glide angle and it is just a different expression of L/D ratio.

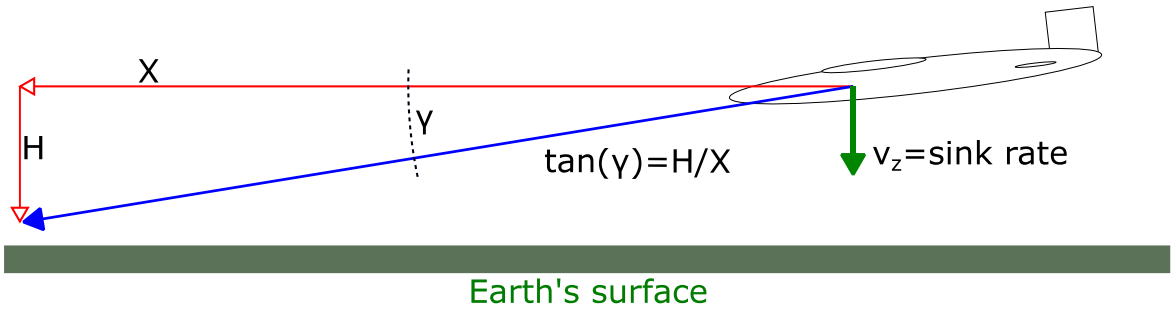

Figure 3: Glide Ratio and Rate of Sink

Rate of sink is a downward velocity of the aircraft with respect to Earth while flying in homogeneous air of zero wind velocity. Flying at the minimum sink rate is desirable especially in situations with goals based on the total amount of time spent in the air, in which the endurance is crucial. It is also desirable to fly at minimum sink rate in thermals to maximize the gained altitude.

2.3 LIFT AND DRAG FORCES

Gliding performance is affected by lift and drag forces. The mass of the aircraft is the cause for gravitational force. The vector of gravitational force always points down to the Earth's surface. The gravitational force is being compensated by lift force. The resulting lift force is a sum of lift of the

wing, lift of the horizontal tailplane, and lift of other components like fuselage. The lift forces acts through the centers of pressure of the wing or horizontal stabilizer respectively [4]. The last force discussed and dealt with in this section is the drag. The drag plays a crucial role in both L/D ratio and the rate of sink. To maximize flying range of the aircraft, it is desirable to fly at angle of attack (AoA) for the maximum L/D ratio, increasing the lift while keeping the drag minimal.

While the center of pressure moves with AoA, the moment of the lift force is constant with respect to aerodynamic center. In a steady flight, the pitching moment is zero with respect to CoG of the aircraft. This is achieved when lift force of horizontal stabilizer compensates the moment of lift force of the wing. The aircraft rotates around its CoG. When the CoG is shifted, the moment also changes and a modified elevator trimming is required to balance the difference.

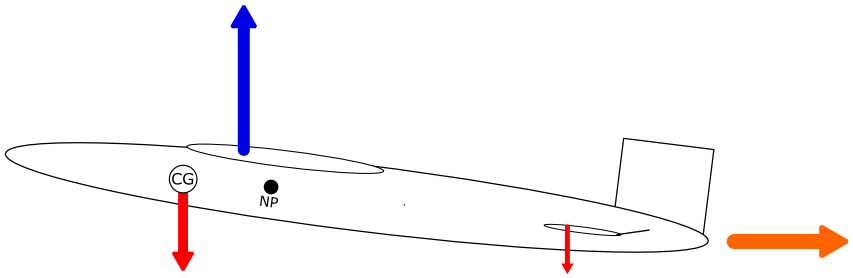

Figure 4: Forces acting on an Aircraft with a Big Positive Stability Margin

FIGURE 4 shows a case in which the CoG is located far to the front of the Neutral Point (NP). This configuration provides a big positive margin of longitudinal stability. The moment of the wing's lift is compensated by downward lift force of the horizontal stabilizer. To fully compensate the gravitational force, lift of the wing must be sufficient to counteract the negative lift of the tailplane, resulting in higher AoA and an increased drag. Although this configuration creates a huge stability margin, it is not a viable option for a performance flight due to the increased drag and lift loss at the tailplane.

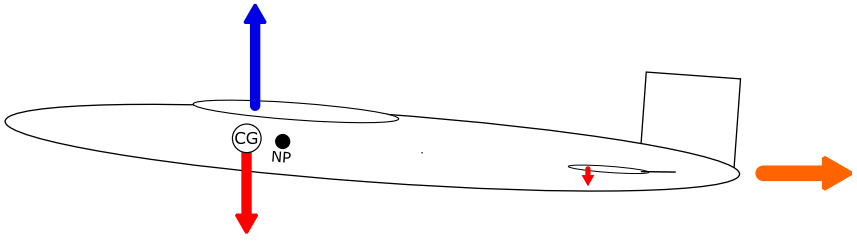

Figure 5: Forces acting on an Aircraft with a Small Positive Stability Margin

In FIGURE 5, the CoG is moved towards the NP. The stability margin in this case is sufficient to keep the aircraft stable. The compensation of the moment of the wing is considerably smaller than in the previous case. The wing compensates less downward lift of the tail which results in less drag. This configuration is widely used because of the acceptable performance as well as the controllability by a human pilot.

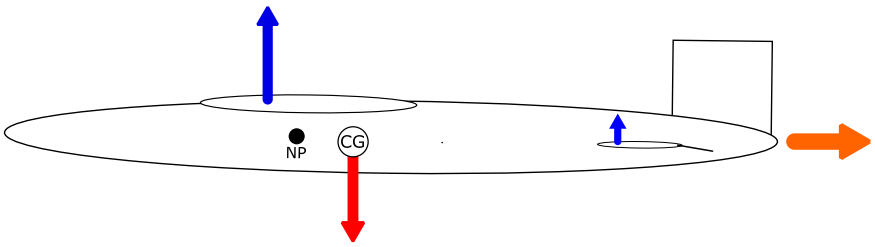

Figure 6: Forces acting on an Aircraft with a Negative Stability Margin

The proposed solution closely investigated in chapters 6 and 7 has a longitudinal stability reduced. The increased pitching moment of the wing is compensated by a positive lift of the tail. Gravitational force is compensated while flying at lower AoA while causing less induced drag. This situation is pictured in FIGURE 6.

3 MODULAR TESTBED AIRCRAFT

To carry out the tests proposed later in this thesis, a custom RC testbed aircraft (FIGURE 7) has been made. Since the characteristics of this aircraft play a major role in the simulation and verification tests, it is important to introduce the plane and describe it in detail.

Figure 7: The Testbed Aircraft with most Rear position of the Tailplane

3.1 MODULARITY AND CONSTRUCTION

To ensure possibility of wide range of airborne tests of longitudinal and lateral properties of the aircraft, structure needs to be modular. This way, the aerodynamic characteristics change with the changed structure and so do the flight properties. Aircraft modularity requirements were following:

- Movable position of horizontal and vertical stabilizer on rear fuselage
- Changeable wing dihedral
- Movable center of gravity
- Adjustable vertical position of the wing
- Movable position of the motor

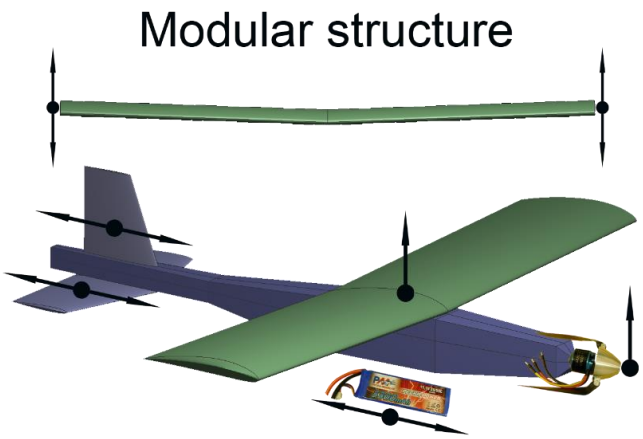

Figure 8: Modular Structure Scheme

Planned modular structure can be observed in **FIGURE 8**. This plan was fulfilled except of upward shift of the wing and similar possibility for the motor, which exceeds the extent of this thesis and will be added in future. Modular parts are described in following paragraphs.

3.1.1 HORIZONTAL AND VERTICAL STABILIZERS

Figure 9: Tailplane Mount and Rudder Servo Placement

The separate movable horizontal and vertical stabilizer was achieved by mounting each element to the other side of the aircraft fuselage. Specifically, horizontal tailplane was chosen to mount on the downward side and vertical tailplane to the upward one. To secure the sustainability, both components are mounted to the fuselage by rubber bands.

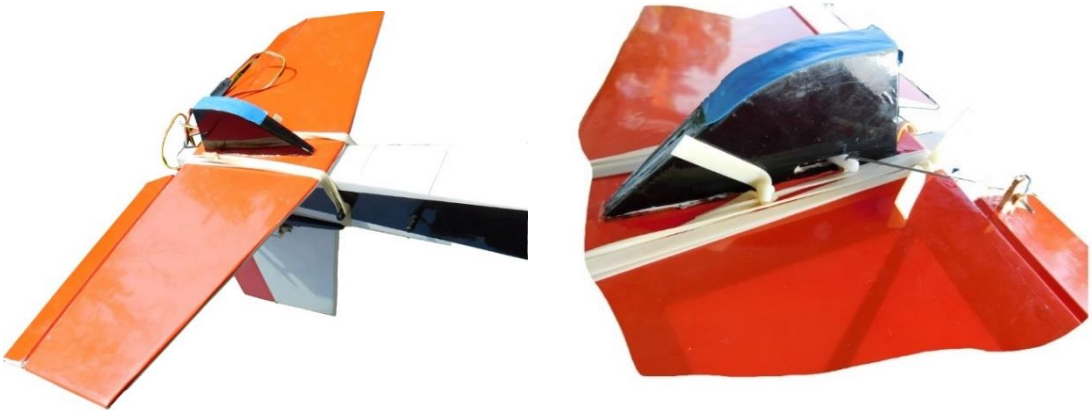

Figure 10: Horizontal Stabilizer Mount to the Bottom of Rear Fuselage and Elevator Servo Mount

To enable the modularity, servos to move the control surfaces are mounted to the tail surfaces. The vertical stabilizer servo is glued directly to the fin. The horizontal stabilizer's control element is mount to the fin pointing down as shown in **FIGURE 10** that also protects the elevator from damage during landing phase.

3.1.2 CHANGEABLE DIHEDRAL

Changeable wing dihedral affects longitudinal motion insignificantly. However, when doing flying tests, it is not desired to deal with the issues of unstable lateral modes. As for the dihedral values, it was chosen to have dihedral possibilities of 0, 2, and 4 degrees. The last value should establish spiral stability of the lateral mode and ensure focus on longitudinal dynamics. However, field tests showed that stability should be better achieved by additional roll controller.

Figure 11: Changeable Dihedral - 2, 0, and 4 degrees

The change of dihedral was made as simple as possible in terms of additional components of the structure. To use one connecting rod for both sides of the wing, few holes of different angles were drilled in early stages of the building process as shown in FIGURE 11.

3.1.3 CENTER OF GRAVITY

The change of this parameter can be achieved by moving non-structural part of the airplane. The heaviest and the most movable part of the airplane is the battery. To ensure the the battery can be moved easily, the fuselage is made spacious enough to store the autopilot electronics comfortably with any position of the battery. Interior of the fuselage can be seen in FIGURE 12.

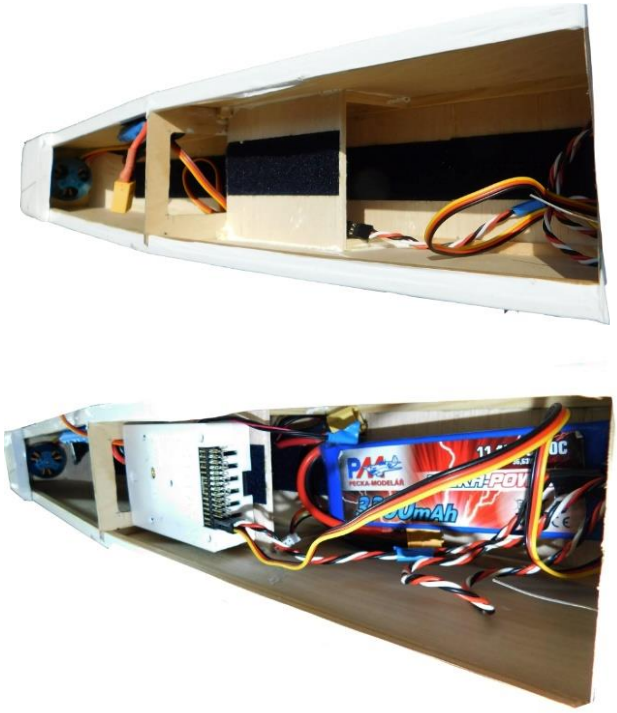

Figure 12: Spacious Fuselage with Velcro stripes and component placement

3.2 SPECIFICATIONS

Each part of the aircraft was weighted on scales with precision of 1 gram. The weight of components is shown in the following TABLE 1. All components are used in computation of the moment of inertia as well as the center of gravity of the aircraft.

part	*grams*	*quantity*	*total kg*
Spinner + propeller	35	1	0,035
Motor	107	1	0,107
Speed controller	59	1	0,059
Receiver	14	1	0,014
Battery	250	1	0,25
Servo	10	4	0,04
Extending cables – short	4	2	0,008
Extending cables – long	15	2	0,03
Navio+raspberry+cable+case+gps	171	1	0,175
Wing	169	2	0,338
Wing connecting rod	50	1	0,05
Horizontal stabilizer	45	1	0,045
Vertical stabilizer	17	1	0,017
Fuselage	347	1	0,347
	TOTAL WEIGHT		**1,511 kg**
	STRUCTURE WEIGHT		0,797 kg

Table 1: Testbed Aircraft Component Overview

The actual testbed aircraft specifications are described in TABLE 2.

Parameter	Value	Unit
Wing airfoil	NACA 4412	
Wingspan	1,2	m
Aerodynamic chord	0,25	m
Wing area	0,3	m^2
Wing loading	5,05	kg/m^2
Weight (without autopilot)	1,34	kg
Weight (full)	1,51	kg
Battery capacity	3300	mAh

Table 2: Testbed Aircraft Specifications

3.3 CONFIGURATION DETERMINATION

To improve understanding of the rest of this thesis, a guide to aircraft's configuration determination is presented in this section. Since it is dealt with longitudinal dynamics, the main axis along which are the components shifted is x or $roll$ axis of the airplane. To unify the locations, a reference point must be set. x location of the leading edge of the aircraft has been chosen as a reference point in all tests. Component location is always determined as a subtraction of location of this reference point

and the most forward position of the component. This way, an axis with the origin at x coordinate of the leading edge of the wing with positive values towards the tail is established.

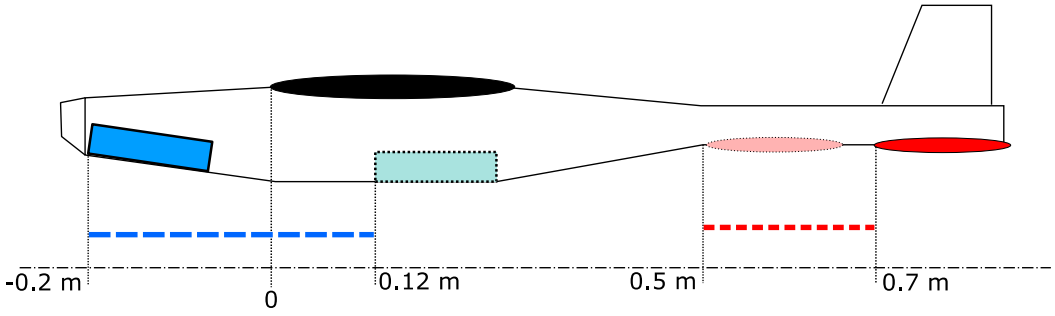

Figure 13: Possible Positions for Battery and Horizontal Stabilizer

Two components of the airplane are moved during the tests. The movability can be seen in FIGURE 13. Horizontal stabilizer affects the aircraft appearance as well as its aerodynamic characteristics. There are four possible locations of horizontal stabilizer:

$$x = \{0.5\ m; 0.55\ m; 0.65\ m; 0.7\ m\}. \quad (1)$$

Second movable component is the battery, that can be shifted in range of

$$x =< -0.2\ m; 0.12\ m >. \quad (2)$$

These shifts contribute to the change of CoG proportionally to the shift and the weight of the components.

3.4 HARDWARE IMPLEMENTATION

Figure 14: Raspberry PI 3 + Navio 2 Protection Case (3D printed)

The chosen hardware is a set of Raspberry PI 3 Model B and Navio 2. To keep the hardware safe from mechanical damage, a protection case was 3D printed. Additionally, the hardware is mount in the airplane with a stripe of Velcro, what eliminates significantly more vibrations than a hard screw mount.

3.4.1 SENSORIC SETS

Flight parameters are measured by sensors that are default for the mentioned devices. The inertial measurement units (IMU) are two nine-degree-of-freedom sensors – MPU9250 and LSM9DS1. Each of them contains an accelerometer, gyroscope and magnetometer. Every sensoric part measures along 3 axes. Specifications stated by manufacturer are:

Barometer sensor is MS5611-01BA03, which provides temperature and static pressure measurements. Specifications of this sensor are shown in TABLE 3.

Sensor Performances (V_{DD} = 3 V)				
Pressure	**Min**	**Typ**	**Max**	**Unit**
Range	10		1200	mbar
ADC		24		bit
Resolution (1)		0.065 / 0.042 / 0.027 / 0.018 / 0.012		mbar
Accuracy 25°C, 750 mbar	-1.5		+1.5	mbar
Error band, -20°C to +85°C 450 to 1100 mbar (2)	-2.5		+2.5	mbar
Response time (1)		0.5 / 1.1 / 2.1 / 4.1 / 8.22		ms
Long term stability		±1		mbar/yr
Temperature	**Min**	**Typ**	**Max**	**Unit**
Range	-40		+85	°C
Resolution		<0.01		°C
Accuracy	-0.8		+0.8	°C
Notes: (1) Oversampling Ratio: 256 / 512 / 1024 / 2048 / 4096 (2) With autozero at one pressure point				

Table 3: Data Sheet of Barometer

To get satisfying frequency of barometer measurements, the oversampling ratio was set to 512.

The GPS module NEO-M8N is connected over SPI, and sends navigation messages and configuration data. Performance of this component can be found in TABLE 4.

Parameter	Specification	Value
Receiver type	*2-channel u-blox M8 engine* *GPS L1C/A* *SBAS L1C/A* *QZSS L1C/A* *GLONASS L1OF* *BeiDou B1* *Galileo E1B/C*	
Horizontal position accuracy	*Autonomous*	2.5 m
	SBAS	2.0 m
Time-To-First-Fix	*Cold start*	29 s
	Hot start	1 s
Max navigation update rate		10 Hz

Table 4: Data Sheet of Ublox GNSS Module

The GPS module provides the following output:

- Latitude
- Longitude
- Computed horizontal accuracy
- Altitude (ellipsoid)
- Altitude (MSL)
- Computed vertical accuracy

3.4.2 DATA ACQUISITION

For the needs of quantitative results, a custom data-acquisition application was programmed. The computational unit runs a program that is designed to stabilize the aircraft at set pitch or roll angle. To ensure a smooth run and desirable frequency, four threads are utilized. The first obtains data from IMUs and writes the general telemetry data to a file with a desired frequency of 130Hz. This main thread uses two additional threads to read data from gps and barometer. These three threads are not prioritized over the standard threads. The last thread runs with real-time priority. This thread secures the control and stabilization of the aircraft as well as transfer of the inputs from the receiver to servos. Besides that, control input and output data are also saved to a file. The desired frequency of the control is 100Hz. The frequency exceeds the frequency of the PWM by a safety margin in

case of any frequency drops. It happened several times during few hours of performance tests, but never dropped under 70Hz.

The computational unit saves data in two files. One contains general flight data and the other one contains data related to the control laws and the control itself. The first file's structure is:

$$time \mid attitude\ angles \mid angular\ rates \mid IMU1\ data \mid IMU2\ data \mid Barometer\ data \mid GPS\ data$$

The second file contains the following parameters:

$$time \mid motor \mid rudder \mid attitude\ angles \mid control\ in \mid control\ out$$

Only attitude angles are being calculated onboard, what is demanded by the control system. The calculations use the Mahony AHRS algorithm [5] based on quaternions. The input is supplied with data from MPU9250. The rest of the parameters is computed during postprocessing.

The parameters needed for deeper analysis are post-processed after the flight. As the object of interest is the flight performance, data processing is oriented to get the position and altitude in time. It is required to choose the relevant sections of the flight. This can be done by reviewing flight data with respect to the attitude angles and control inputs or outputs respectively. This process is described in Chapter 7.

4 LONGITUDINAL DYNAMICS

In this chapter, mathematical model of an aircraft is presented. The first part describes basic principles. The second part is focused on getting an accurate model for the testbed aircraft presented in Chapter 3. The model considers aerodynamic coefficients and inertia. The third part describes the trimming laws and investigates longitudinal stability.

4.1 BASIC PRINCIPLES

4.1.1 COORDINATE SYSTEMS

Before describing the basic principles of movement, several different reference systems must be introduced. Since it is dealt just with the longitudinal part of aircraft mechanics, every reference system is simplified to two axes of translational movement, x and z, and one axis of rotation, y. The systems can be divided into two categories; body-fixed and earth coordinate systems [6].

The body-fixed coordinate systems for an aircraft used in this thesis and displayed in FIGURE 15 are:

- Body axes
- Stability axes
- Earth axes - NED

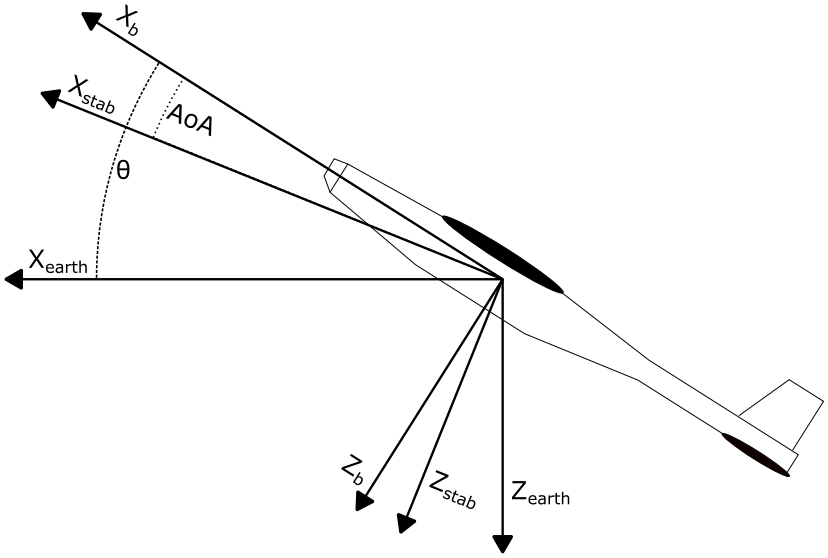

Figure 15: Body, Stability, and Earth Coordinate Systems

These coordinate systems are related to each other by angles θ between NED and body reference systems and α between stability and body reference systems. The rotational matrices to transform vectors between the reference systems are

$$R_{body}^{ned} = \begin{bmatrix} \cos(\theta) & \sin(\theta) \\ -\sin(\theta) & \cos(\theta) \end{bmatrix}, \quad (3)$$

$$R_{body}^{stab} = \begin{bmatrix} \cos(\alpha) & \sin(\alpha) \\ -\sin(\alpha) & \cos(\alpha) \end{bmatrix}. \quad (4)$$

4.1.2 AIRCRAFT STATE-SPACE VECTORS

In the description of the mathematic model, the definitions of movements and positions in TABLE 5 are used later in this thesis.

Symbol	Meaning
U	Longitudinal velocity
W	Vertical velocity
Q	Pitch rate
R	Pitch rate
X_e	x-coordinate in Earth coordinate system
Z_e	z-coordinate in Earth coordinate system
θ	Pitch attitude
ϕ	Roll attitude
α	Angle of Attack

Table 5: Movement and position definition

Forces and moment used in the longitudinal dynamics modelling are listed in TABLE 6.

Symbol	Meaning
X	Longitudinal force
Z	Vertical force
M	Pitching moment

Table 6: Forces and moment definition

The transformation parameter is angle of attack, which is defined as

$$\tan(\alpha) = \frac{W}{U}. \quad (5)$$

4.1.3 KINEMATIC EQUATION OF LONGITUDINAL MOTION

Kinematic equations for translation in earth coordinates can be described by velocities transformed from body to earth coordinates as follows:

$$\begin{bmatrix} \dot{X}_e \\ \dot{Z}_e \end{bmatrix} = R_{body}^{ned} \begin{bmatrix} U \\ W \end{bmatrix} = \begin{bmatrix} \cos(\theta) & \sin(\theta) \\ -\sin(\theta) & \cos(\theta) \end{bmatrix} \begin{bmatrix} U \\ W \end{bmatrix}. \quad (6)$$

That results in equations

$$\dot{X}_e = cos(\theta)U + sin(\theta)W, \quad (7)$$

$$\dot{Z}_e = cos(\theta)W - sin(\theta)U. \quad (8)$$

Kinematic equation for pitch attitude is simply defined as

$$Q = \dot{\theta}. \quad (9)$$

4.1.4 DYNAMICS OF RIGID-BODY AIRCRAFT

Dynamics of rigid-body aircraft in component form is described in body coordinate system, that is assumed to be in the center of gravity of the aircraft. Definition of the dynamics is

$$X = m(\dot{U} + QW), \quad (10)$$

$$Z = m(\dot{W} - QU), \quad (11)$$

$$M = I_y \dot{Q}. \quad (12)$$

where I_y is a moment of inertia along the y (lateral) axis.

Forces in component form can be written as a composition of aerodynamic forces and force caused by gravity. Considering dynamic pressure being (13) and thrust being T_x , the equations describing the forces have the following form:

$$\bar{q} = \frac{1}{2}\rho v^2 \quad (13)$$

$$\vec{F} = \vec{F}_{aero} + \begin{bmatrix} T_x \\ 0 \end{bmatrix} + \vec{F}_g, \quad (14)$$

$$F_{aero} = \begin{bmatrix} \bar{q}SC_x \\ \bar{q}SC_z \end{bmatrix}, \tag{15}$$

$$\vec{F} = \begin{bmatrix} \bar{q}SC_x + T_x - m \cdot g \cdot sin(\theta) \\ \bar{q}SC_z + m \cdot g \cdot cos(\theta) \end{bmatrix} = \mathrm{m} \begin{bmatrix} \dot{U} + QW \\ \dot{W} - QU \end{bmatrix}. \tag{16}$$

Similarly, the moment of aerodynamic forces along lateral axis can be defined as a sum of moment of aerodynamic forces in neutral point and additional moment of lift force caused by center of gravity location not being the same as the location of neutral point.

$$M_{aero} = \bar{q}S\bar{c}C_M, \tag{17}$$

$$M_{body} = M_{aero_{NP}} + M_{F_z} = \bar{q}S\bar{c}C_{M_{NP}} + \bar{q}SC_L(r_{NP} - r_{CG}), \tag{18}$$

where $\bar{q}$ is a dynamic pressure, S wing area, and $\bar{c}$ mean aerodynamic chord.

Because drag and lift coefficients describe forces in back and up coordinates, negative transformed value of these coefficients must be used.

$$\begin{bmatrix} C_x \\ C_z \end{bmatrix} = -R_{stab}^{body} \begin{bmatrix} C_D \\ C_L \end{bmatrix} \tag{19}$$

Acceleration in body coordinates can be expressed as a sum of acceleration caused by aerodynamic forces and gravitational acceleration transformed from earth to body coordinate system.

$$\vec{a}_{body} = \vec{a}_{aero} + \vec{a}_g = \begin{bmatrix} \frac{\bar{q}SC_x}{m} - g \cdot sin(\theta) \\ \frac{\bar{q}SC_z}{m} + g \cdot cos(\theta) \end{bmatrix} \tag{20}$$

For the Q, similarly to the translational accelerations, can be written:

$$\frac{M_{body}}{I_y} = \dot{Q}, \tag{21}$$

where I_y represents moment of inertia around lateral axis.

For the translational speeds along x and z axes from equation (xx)

$$a_{x_{body}} - QW = \dot{U} \tag{22}$$

$$a_{y_{body}} + QU = \dot{W} \tag{23}$$

4.2 AERODYNAMIC COEFFICIENTS

There are three types of aerodynamic coefficients that influence an accurate mathematic model of an aircraft:

- Static coefficients C_{X_0} , C_{X_α}, $C_{X_{\alpha^2}}$ are applicable for static conditions. As a simple linear approximation is not enough accurate to model the aircraft with all its properties, the approximation is done by 2nd degree polynomial.

- Control coefficient $C_{X_{\delta e}}$ applies, when the control surface, which is elevator in this case, deflects by δe. In case of drag, induced drag is computed.

$$C_{D_{\delta e}} = \frac{\left(C_{L_{\delta e}} \cdot \delta e\right)^2}{\pi \cdot AR \cdot e} \tag{24}$$

  Symbol e represents span efficiency factor and AR represents aspect ratio. [7]

- Dynamic coefficient C_{X_Q} is applied, when the aircraft changes its attitude, in other words Q is not equal to zero. The dynamic component is then dependent on dynamic pressure $\bar{q}$, mean aerodynamic chord $\bar{c}$, and airspeed v.

The equations to compute the coefficients are:

$$C_D = C_{D_0} + C_{D_\alpha} \cdot \alpha + C_{D_{\alpha^2}} \cdot \alpha^2 + \frac{\left(C_{L_{\delta e}} \cdot \delta e\right)^2}{\pi \cdot AR_{stab} \cdot e}, \tag{25}$$

$$C_L = C_{L_0} + C_{L_\alpha} \cdot \alpha + C_{L_{\alpha^2}} \cdot \alpha^2 + C_{L_{\delta e}} \cdot \delta e + C_{L_Q} \cdot \frac{Q\bar{c}}{2v}, \tag{26}$$

$$C_m = C_{m_0} + C_{m_\alpha} \cdot \alpha + C_{m_{\alpha^2}} \cdot \alpha^2 + C_{m_{\delta e}} \cdot \delta e + C_{m_Q} \cdot \frac{Q\bar{c}}{2v}. \tag{27}$$

These coefficients are computed from aerodynamic simulations in programs **xflr5**[1] and **AVL**[2] .

As the modelled aircraft is modular, a simple look-up table was made. After the desired configuration is known, the mathematical model finds appropriate coefficients for the chosen aerodynamic configuration.

[1] For aerodynamic simulations, Vortex Lattice Method (VLM) was used. See http://www.xflr5.com/xflr5.htm for more information about xflr5 simulator.
[2] AVL's Extended Vortex-Lattice Model was used to obtain aerodynamic coefficients for control and dynamic coefficients related to pitch rate. See http://web.mit.edu/drela/Public/web/avl/ for more information about AVL.

4.3 MOMENT OF INERTIA CALCULATION

Since the investigated aircraft is modular, inertial calculation is not same for every configuration. Final moment of inertia is a sum of moments of inertia of separate components that are listed in Table 1. These comprise of two parts. The first part describes the rotation with respect to axis that goes through the center of gravity of the component. The second part uses Steiner's theorem $I_{tot} = I_{cm} + md^2$, and reflects the moment of inertia about the axis, that is going through the center of gravity of the entire aircraft.

To get the precise values, every component was investigated for its weight, center of gravity, and when non-homogenous in density, even estimated real moment of inertia.

4.4 TRIMMING

To proceed to system linearization, it is needed to trim the model to a steady position. This can be achieved by solving several motion equations, which are the following.

1. Trimming in the best glide ratio (28) at $\max\left(\frac{C_L}{C_D}\right)$ or minimum sink rate (29) at $\max\left(\frac{C_L^{3/2}}{C_D}\right)$:

$$\frac{d\left(\frac{C_{L_{trim}}(\alpha)}{C_{D_{trim}}(\alpha)}\right)}{d\alpha} = 0, \qquad \alpha \in < -5; 15 > \tag{28}$$

$$\frac{d\left(\frac{C_{L_{trim}}^{3/2}(\alpha)}{C_{D_{trim}}(\alpha)}\right)}{d\alpha} = 0, \qquad \alpha \in < -5; 15 > \tag{29}$$

2. Lift equation:

$$C_{L_{trim}} = \frac{\cos(\alpha_{trim} - \theta_{trim})\, mg - T \cdot \sin(\alpha_{trim})}{\frac{1}{2}\rho v^2 S} = C_{L_0} + C_{L_\alpha} \cdot \alpha_{trim} + C_{L_{\alpha^2}} \cdot \alpha_{trim}^2 + C_{L_{\delta e}} \cdot \delta e_{trim} \tag{30}$$

3. Drag equation:

$$C_{D_{trim}} = C_{D_0} + C_{D_\alpha} \cdot \alpha_{trim} + C_{D_{\alpha^2}} \cdot {\alpha_{trim}}^2 + \frac{\left(C_{L_{\delta e}} \cdot \delta e_{trim}\right)^2}{\pi \cdot AR_{stab} \cdot e} \tag{31}$$

4. Total coefficient along x – axis of stability axes:

$$\mathrm{C_{D_{tot}}} = C_{D_{trim}} - T_x \cdot \frac{\cos(\alpha_{trim})}{\frac{1}{2}\rho v^2 S} \tag{32}$$

5. Zero moment equation:

$$0 = C_{m_{0_{AC}}} + C_{m_{\alpha_{AC}}} \cdot \alpha_{trim} + C_{m_{\alpha^2{}_{AC}}} \cdot {\alpha_{trim}}^2 + C_{m_{\delta e_{AC}}} \cdot \delta e_{trim} - \frac{NP - CoG}{c}\left(C_{L_0} + C_{L_\alpha} \cdot \alpha_{trim} + C_{L_{\alpha^2}} \cdot \alpha_{trim}^2 + C_{L_{\delta e}} \cdot \delta e_{trim}\right) \tag{33}$$

6. Pitch equation that computes pitch as a difference of α_{trim} and glide slope γ:

$$\theta_{trim} = \alpha_{trim} - \gamma_{trim} = \alpha_{trim} - \arctan\left(\frac{C_D}{C_L}\right) \tag{34}$$

7. The trimming itself also counts on user interaction, so it is needed to specify, whether the aircraft model should be trimmed to glide without a thrust, therefore $T = 0$, or to fly steadily with zero glide slope which implies the drag is compensated by the thrust, therefore $\mathrm{C_{D_{tot}}} = 0$.

4.5 LINEARIZATION AND STABILITY

The described nonlinear aircraft dynamical system is very complicated in terms of control analysis. For the control design, it is advantageous to work with a system that is a linearization of the sophisticated nonlinear system around the equilibrium point. Such linearization can replace the nonlinear system around the vicinity of the equilibrium point and keeps the behavior of the linearized system – the effect of a small perturbation away from the equilibrium point can be studied; e.g. whether the perturbation grows or decreases.

As for the general aircraft longitudinal linear model, the denominator of the transfer function describes the modal properties of the system. In general, there are two longitudinal modes, a phugoid mode and a short period mode.

In [8], the phugoid mode is described as a "gradual interchange between potential and kinetic energy about some equilibrium altitude and airspeed", meaning it is a motion of slow changes in

airspeed and pitch attitude. Considering the rate of change of these parameters, which is significantly slower than in case of short-period mode, the trajectory of the aircraft is affected mainly by the phugoid mode.

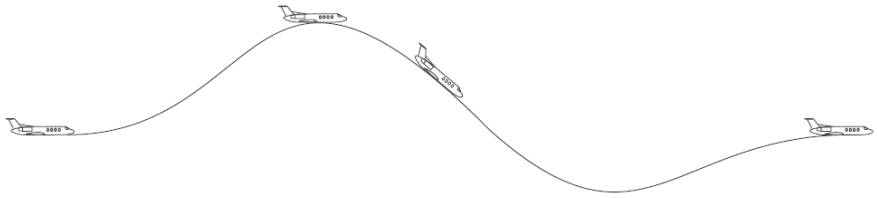

Figure 16: phugoid mode - affecting trajectory (adopted from [8])

The short period mode, however, describes the aircraft's pitching motion around its CoG. As the name describes, this mode has a period of around a tenth of the phugoid mode period. Flight parameters described by short period mode could be obtained from a reaction of the aircraft on elevator deflection – rapid change of the AoA and pitch rate.

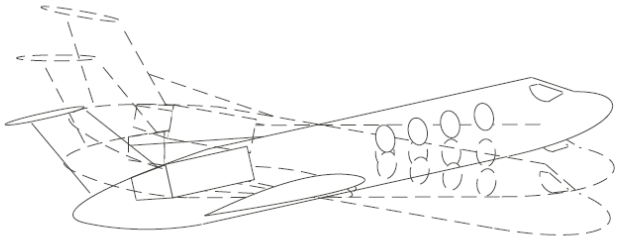

Figure 17: Short Period Mode - causing rotation about CoG (adopted from [8])

The modal analysis is a conventional approach to behavior analysis which fails when analyzing the poles of an aircraft with relaxed static stability. As shown in **FIGURE 18**, poles of the system change dramatically when shifting the center of gravity aft from the initial position.

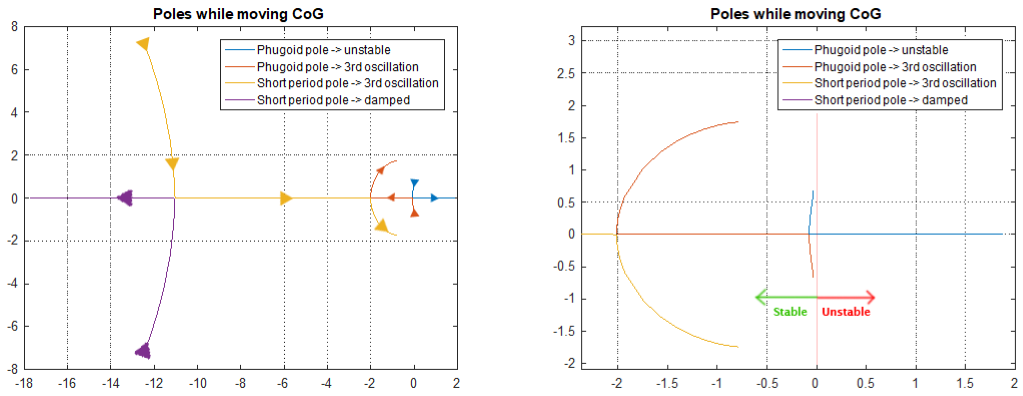

Figure 18: Poles of the longitudinal motion with respect to CoG

Shifting CoG causes five different modal situations that could be considered, as displayed in **FIGURE 19**.

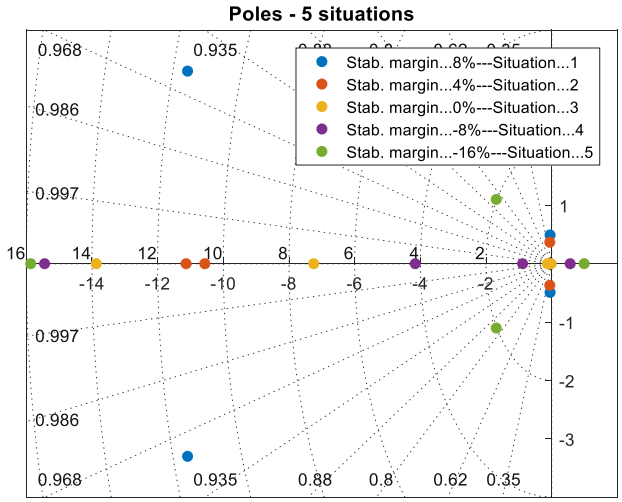

Figure 19: Shifting of CoG and the resulting situations

1. The first situation could be a conventional aircraft with a CoG in highly stable position with respect to the Neutral Point. At this point, both phugoid and short period modes can be obtained. As the CoG is shifted aft, the damping of both modes increases as the CoG is

shifted towards the neutral point. The impulse and step response of such system can be seen in FIGURE 20, colored blue.

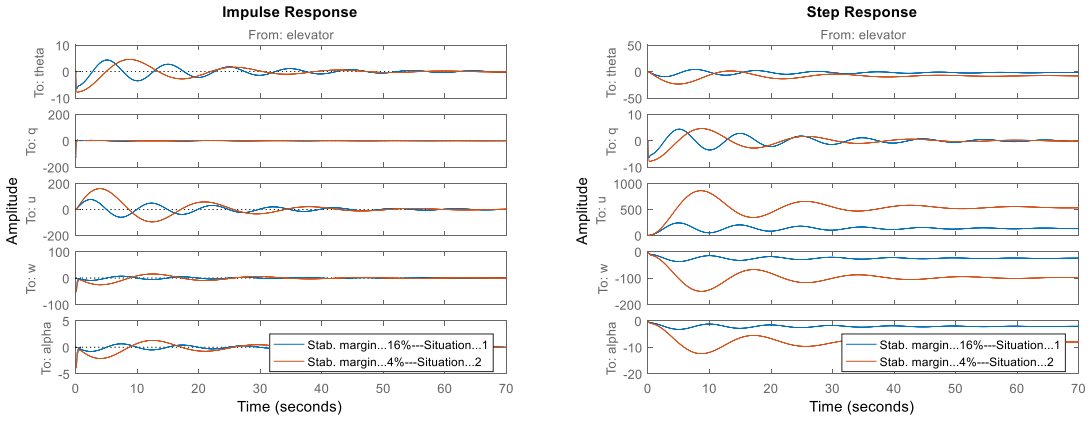

Figure 20: Impulse and Step Response of stable systems

2. Second situation, displayed in red in the FIGURE 20, is the case when the CoG is at a point where the poles of the short period mode get spread on the real axis, while the poles of phugoid mode stay as complex conjugate causing oscillations that are more damped than in the first case. At this stage, the CoG is still located in front of the NP and therefore the aircraft is statically stable.

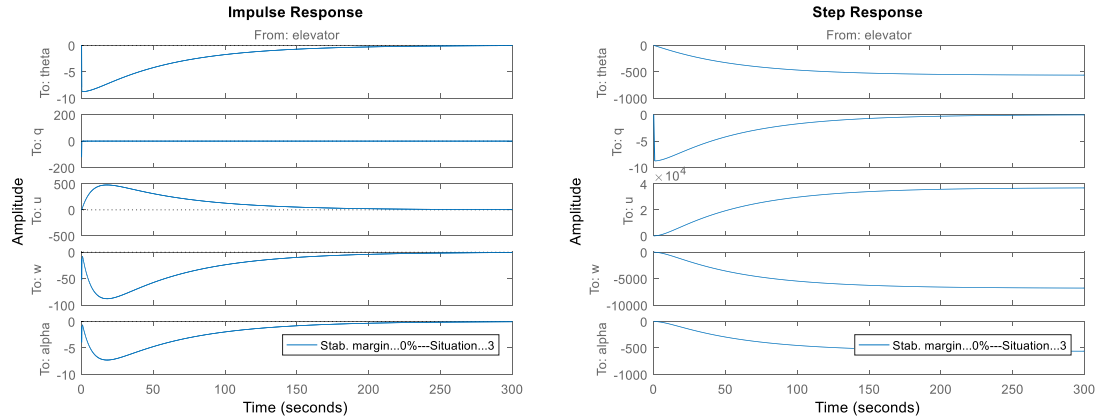

Figure 21: Impulse and Step Response of very low static stability margin

3. Third case includes the CoG located closely in front of the NP that can be considered an edge of stability. In this situation, phugoid mode poles get real and are still of negative values. Therefore, all poles are real and negative and therefore there are no oscillations in the motion of the aircraft while it is being statically stable. This behavior can be seen in FIGURE 21.

4. Fourth position, where the aircraft dynamics differs from the others, is the location of CoG at NP or aft. All poles are real, one of them is zero or positive and therefore the aircraft shows no effort to return to its equilibrium. This is a point, when the aircraft is called statically unstable. Impulse and step response of this situation is displayed in blue color in **FIGURE 22**.

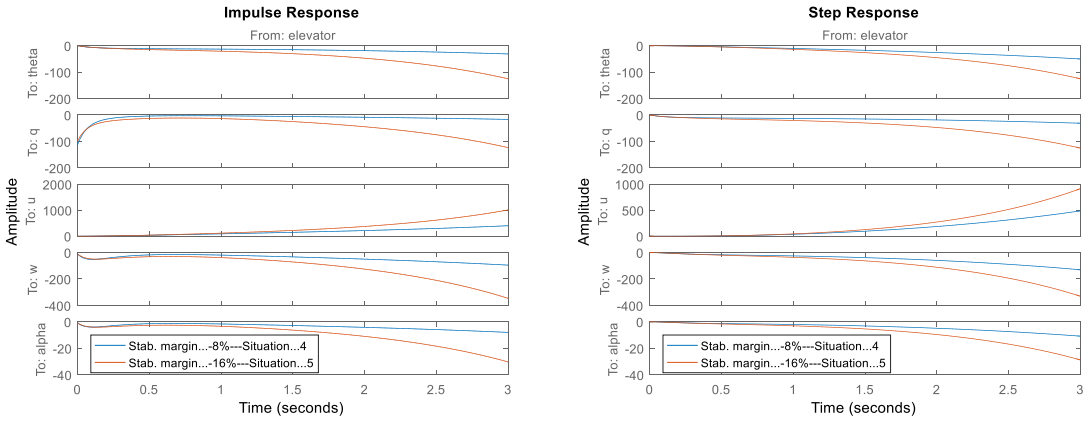

Figure 22: Impulse and Step Response of unstable systems

5. The last case describes a highly unstable aircraft. One of the former short period mode poles causes a "third oscillation" together with one of the former phugoid poles. This oscillation does not affect the unstable behavior in phugoid motion. As **FIGURE 22** shows, the higher instability margin causes a faster grow of the deflection from equilibrium state. The third oscillation causes a difference in dynamic behavior, which is not the objective of this thesis.

As displayed in **FIGURE 23**, poles might also be affected by shifting the horizontal stabilizer forward. The red curve representing the horizontal stabilizer shifted by approximately 30% towards the wing shows significantly lower damping of the short period mode. However, although the change of damping for the short period mode is evident, the characteristics of the phugoid mode remain almost the same.

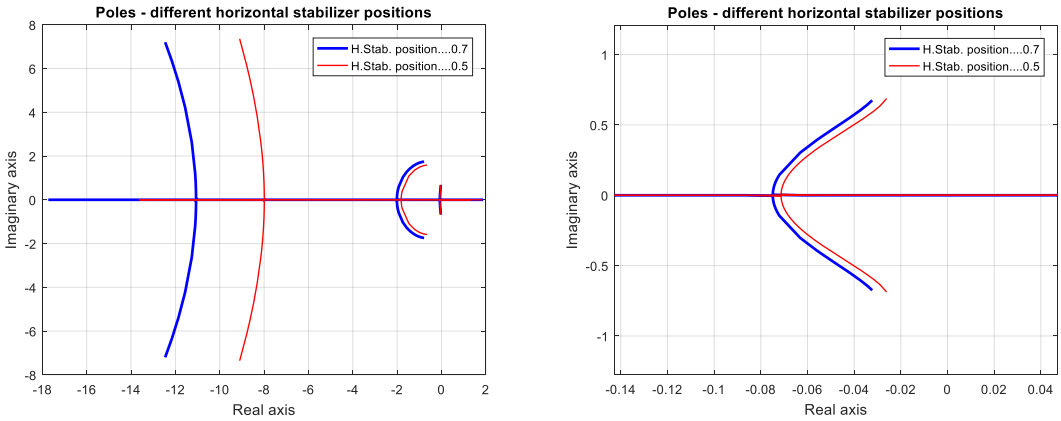

Figure 23: Poles for Different Horizontal Stabilizer positions

The testbed aircraft itself has a limited shift of CoG. Poles corresponding to the positions ranging from the frontest to the rearest possible position are displayed in **FIGURE 24**.

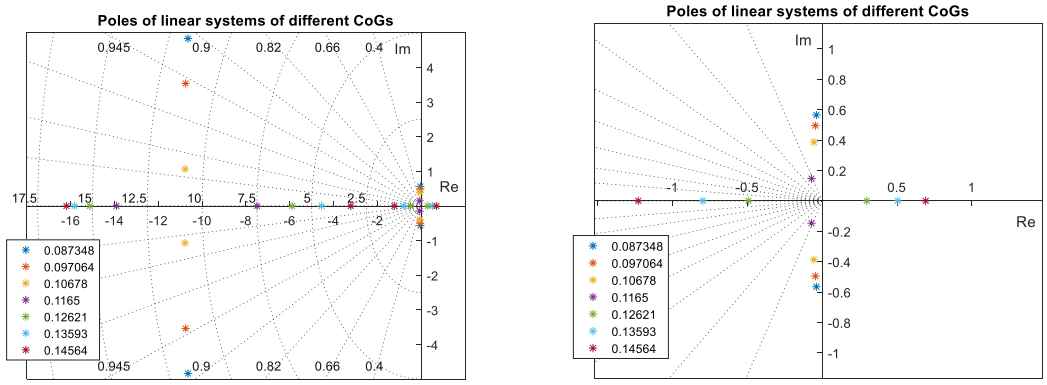

Figure 24: Poles of Testbed Aircraft Dynamic Model

5 AIRCRAFT STABILIZATION AND CONTROL

As briefly introduced in Chapter 2, a statically unstable aircraft needs to be stabilized when it is controlled by a human pilot. Stabilization systems are discussed in this chapter. In the first section, an overview of the existing solutions from available literature is given. Some of the solutions are implemented in MATLAB Simulink and discussed in the second section. The design of the controller to be used in the testbed aircraft concludes this chapter.

5.1 EXISTING SOLUTIONS

5.1.1 DISPLACEMENT AUTOPILOT

According to [9], this type of autopilot has been used in the first aircraft with an autopilot and is still being used in some older types of transport airplanes. The displacement autopilot is designed to hold the airplane in steady flight with pitch attitude being set by the pilot.

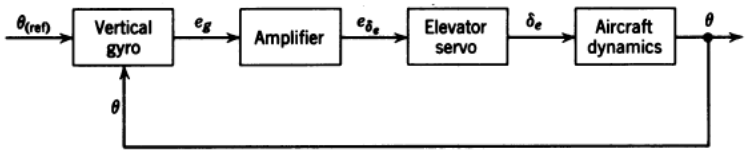

Figure 25: Straightforward Displacement Autopilot (adopted from [9])

The main disadvantage of the control system in FIGURE 25 is the absence of an integrator, a constant external moment causes a constant error in tracking the reference pitch attitude.

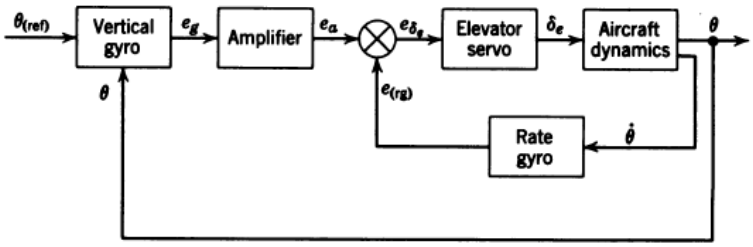

Figure 26: Displacement Autopilot with Pitch Rate Damper (adopted from [9])

While for a conventional slow transport airplane the damping of short period mode for an autopilot without rate gyro damper is sufficient, for a jet transport airplane the damping becomes too low,

which results in dynamic response not being satisfactory. Better damping of the short period oscillations can be achieved by using an inner loop with a rate gyro feedback as shown in FIGURE 26. As the elevator sensitivity is roughly proportional to the speed of flight, in the more advanced controllers the airspeed scaler is added and such system can be seen in FIGURE 27.

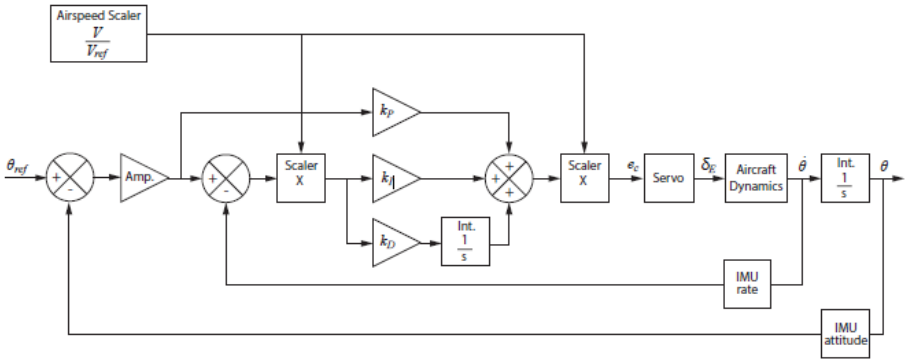

Figure 27: Advanced Displacement Autopilot with Airspeed Scaler (adopted from [10])

5.1.2 PITCH ORIENTATIONAL CONTROL SYSTEM

Pitch orientational system provides precise maneuverability based on setting pitch rate and is widely used in fighter-type aircraft. Input of this control system is a desired pitch rate submitted by the pilot or higher-level control system. The pitch orientational control system contains an integrator that makes it susceptible to the first-order (constant) errors. The utilization of the rate gyro, as well as for the displacement autopilot, depends on the characteristics of the controlled system. [9] It is also stated, that the pitch rate input can be provided by an altitude-mach hold loop or by the pilot himself. The block scheme of such controller can be seen in FIGURE 28.

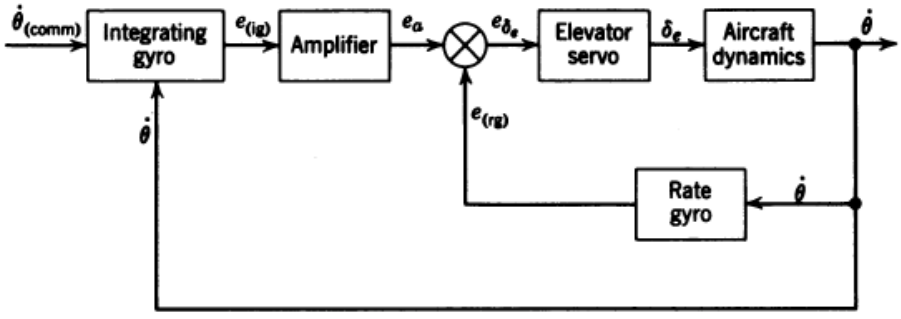

Figure 28: Pitch Orientational Control System (adopted from [9])

There are two types of control sticks: “maneuver stick” that transduces the deflection of the stick to the control elements without any feel to the pilot, and “force stick” that resists the control command with a force proportional to the control deflection. When the stick is released, it comes back to the neutral position with zero desired pitch rate input to the controller. FIGURE 29 shows the whole system being augmented by an airspeed scaler to provide the correct elevator gain for all airspeeds.

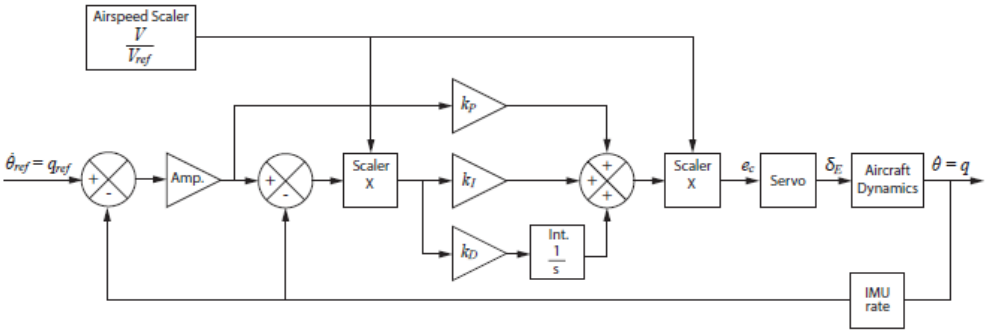

Figure 29: Advanced Pitch Rate Autopilot (adopted from [10])

5.1.3 ACCELERATION CONTROL SYSTEM

According to [9], acceleration control system is a flight control system that is generally used in fighter-type aircraft. An example of use is a maneuver with a quick turn or pitch up at maximum allowable acceleration (load). The block scheme of this autopilot is pictured in FIGURE 30.

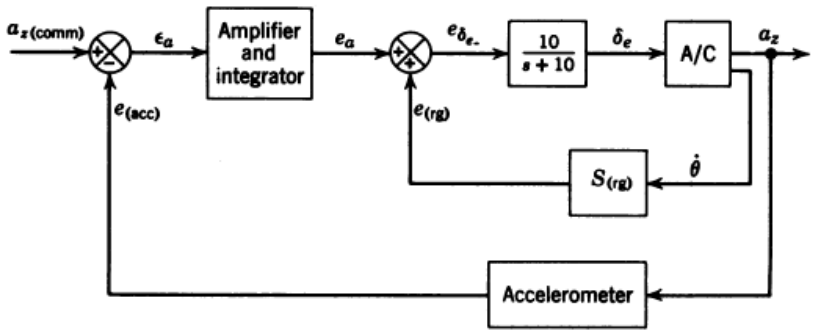

Figure 30: Acceleration Control System (adopted from [9])

The limitation of the system is that an accelerometer cannot distinguish the gravity acceleration and acceleration caused by aircraft motion, for example wind turbulence or simply angle of attack

different from zero. Due to the issues connected to acceleration measurement combined with not many maneuvers that would call for movement at constant acceleration, this flight control system is not often implemented.

5.1.4 ANGLE OF ATTACK CONTROL SYSTEM

All the previous controllers count only on data provided by inertial measurements. Earth-based approach is very convenient to implement and works well in many cases of flight maneuvers. As described in [11], Angle of Attack (AoA) provides significantly more data about the current state of the flight than inertial quantities. With knowledge of AoA, the controller can prevent unwanted stall and therefore increase the safety aspect of a flight, and maximize the flight performance of the aircraft. [10] These are the main reasons, why most of the full-scale aircraft employ the AoA control system. An example of AoA control system with stall limitation and pitch rate damper is shown in FIGURE 31.

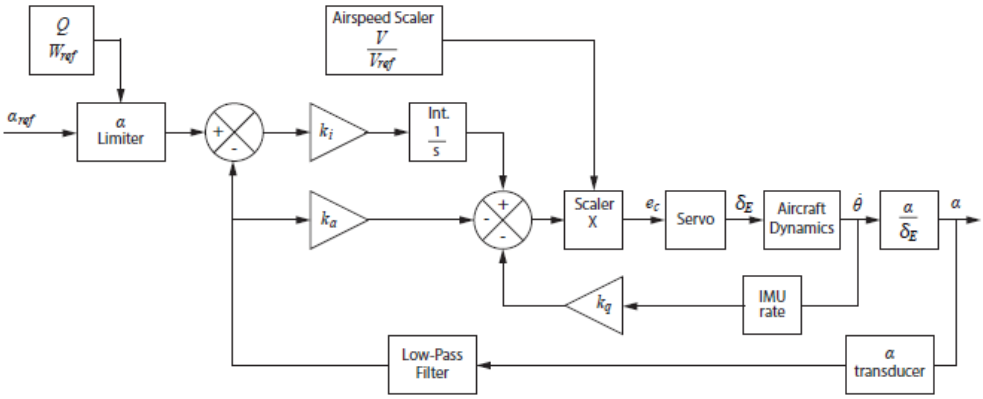

Figure 31: Angle of Attack Control System with Airspeed Scaler (adopted from [10])

The limitation of this flight control system is the precise measurement of AoA. Problems of mechanical measurement of the AoA are described in detail in [11] and it exceeds the extent of this thesis. Most importantly, for sub-scale airplanes, external AoA measurements do not appear to be a viable option of precise acquisition of data for a successful control. Results of experimental AoA measurements on smaller aircraft can be found in [10] or [12].

5.2 IMPLEMENTED LONGITUDINAL CONTROL SYSTEMS

Several controllers have been chosen to be implemented and simulated. Pros and cons discussed above have been verified. Advantages and disadvantages of the pitch rate controller, pitch attitude hold and AoA stabilizer are discussed below.

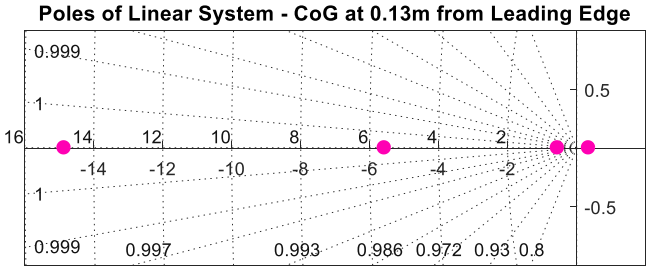

Figure 32: Poles of the System on which Tuning took place

All controllers were tuned on slightly unstable configuration with horizontal stabilizer placed at 0.7 meters from the leading edge of the wing with the neutral point located at 0.117m and the center of gravity at 0.13m. Poles of the linearized model of this system can be seen in FIGURE 32. Effectiveness of the controllers for other CoG locations was investigated as well.

5.2.1 PITCH RATE CONTROLLER

The first tested configuration used a pitch rate controller. This controller has been already described in 5.1.2. Poles of the closed loop for pitch rate feedback to elevator are displayed in FIGURE 33. Feedback from integrated pitch rate to elevator stabilizes the closed loop. Since this is only a proportional feedback, the reference value is not tracked precisely. To track the value precisely, error integration would have to be added.

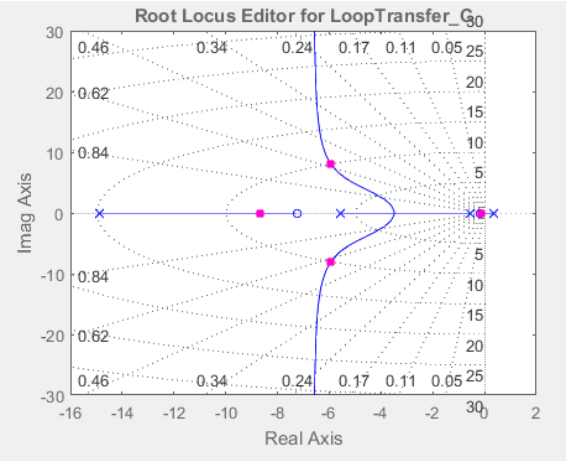

Figure 33: Poles of Closed Loop with Integral of Pitch Rate Feedback

FIGURE 34 shows possible positions of closed-loop poles when the loop includes an integral and proportional feedback based on pitch rate. This loop offers reference tracking as well as stabilization.

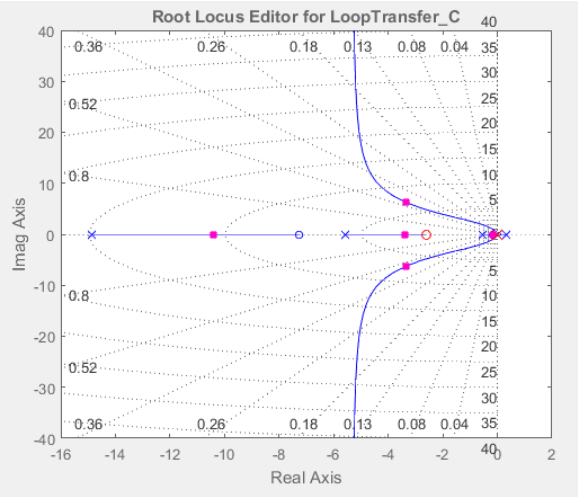

Figure 34: Poles of Closed Loop with Integrated Pitch Rate PI Feedback

The described controller controls pitch rate. Once the airplane is deviated from the state of maximum gliding performance, returning the airplane back to this state is difficult for a human pilot not using higher-level controller. Considering this, the pitch rate autopilot has a limited use in performance gliding. This control strategy is suitable for a fighter-type aircraft where the goal is to perform precise maneuvers.

Controller Parameters

	Tuned
Kp	2.3782
Ki	4.2418
Kd	0.19582
Tf	n/a

Performance and Robustness

	Tuned
Rise time	0.0914 seconds
Settling time	0.919 seconds
Overshoot	7.25 %
Peak	1.07
Gain margin	-43 dB @ 0.368 rad/s
Phase margin	90 deg @ 21.3 rad/s
Closed-loop stability	Stable

Table 7: Tuned Pitch Rate Controller Constants and Performance

Tuned PID controller constants and the controller performance are listed in TABLE 7.

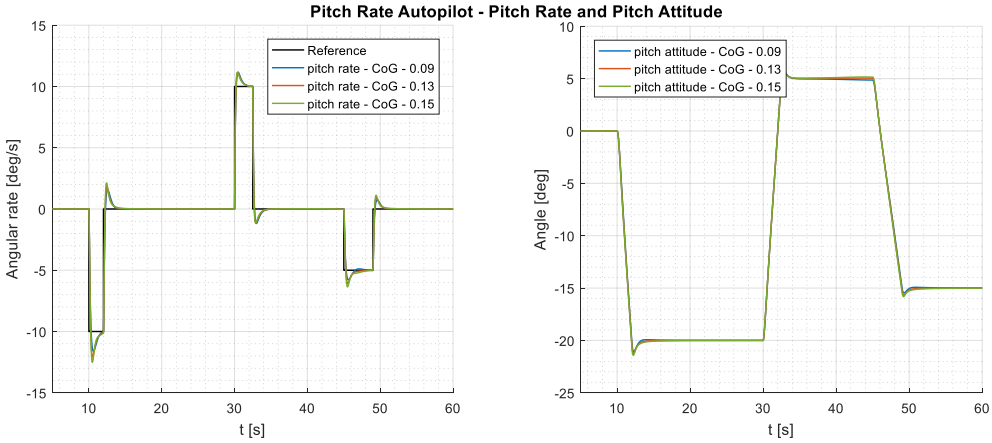

Figure 35: Comparison of Responses of the Closed Loop with PI Pitch Rate Controller for Different CoG Locations

Since the controller has been designed for a slightly unstable configuration, it is required to verify its functionality for other configurations as well to avoid unexpected destabilization that could lead to a crash. This verification can be seen in FIGURE 35. Use of this controller for different configurations does not show much difference in reference tracking and the stability is not affected either.

5.2.2 ANGLE OF ATTACK STABILIZER

The second implemented controller is the angle of attack stabilizer. As shown in FIGURE 36, a direct feedback from AoA to the elevator sets poles of the unstable aircraft similarly to the stable configuration; short period mode as well as stable phugoid mode can be observed. With sufficiently high feedback gain, all poles are in the left half-plane and therefore the aircraft is stabilized.

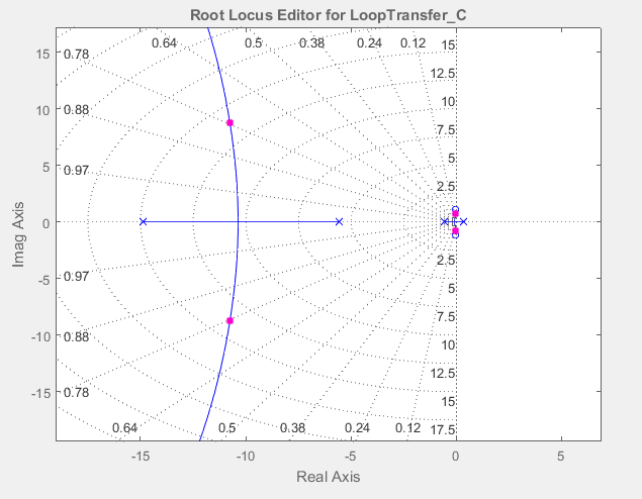

Figure 36: Poles of Closed Loop with AoA Feedback

FIGURE 37 shows the situation when the difference of reference and real AoA is integrated and coupled with the elevator as well as the proportional link. This situation leads to higher gains and a possibility of destabilizing the aircraft in dynamic motion in case of greater imprecisions in AoA measurements.

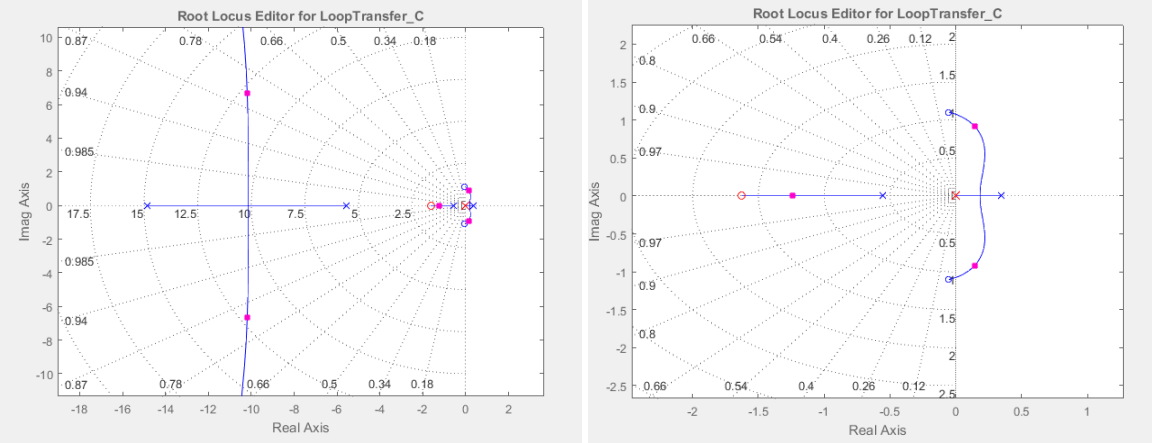

Figure 37: Root Locus of Closed Loop for PI Feedback of AoA

The gains that stabilize the closed loop (as listed in TABLE 8) are quite high and therefore every imprecision is multiplied and integrated to a control error, that might be fatal. This makes the AoA stabilization system alone not very suitable for a small aircraft, where AoA measurements are not so accurate.

Controller Parameters

	Tuned
Kp	25.3426
Ki	354.0018
Kd	0.45356
Tf	n/a

Performance and Robustness

	Tuned
Rise time	0.0255 seconds
Settling time	0.185 seconds
Overshoot	14.7 %
Peak	1.15
Gain margin	-30.7 dB @ 1.11 rad/s
Phase margin	90 deg @ 64 rad/s
Closed-loop stability	Stable

Table 8: Tuned Constants of AoA PID Controller

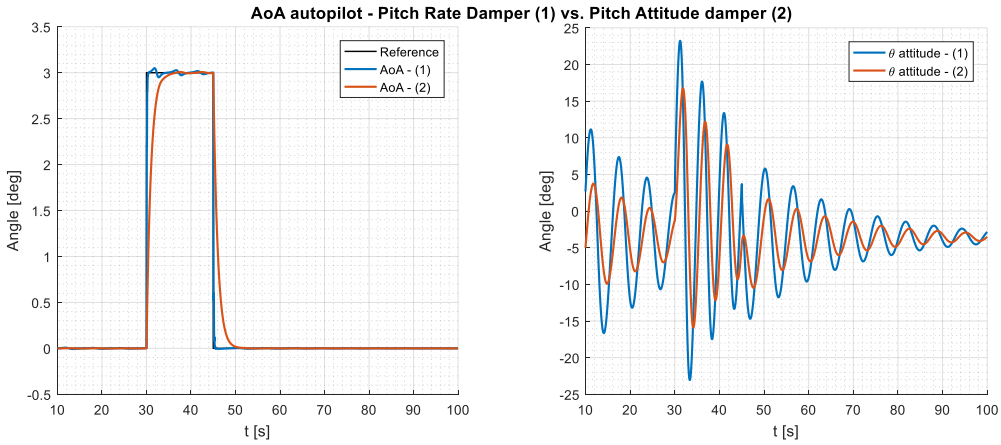

Figure 38: Comparison of AoA Autopilot with Pitch Rate Damping vs. Pitch Attitude Damping

For simulations, the AoA autopilot discussed before in 5.1.4 with block scheme in FIGURE 31 has been implemented. FIGURE 38 shows the reference tracking and the respective pitch attitude of the controller. The autopilot proposed in [10] smoothens the response utilizing a pitch rate damper. However, simulations have shown that a pitch attitude damper provides significantly better damping with slower, but acceptable reference tracking. Since the AoA is stabilized, phugoid mode, where AoA changes only a little, remains almost undamped by the controller which results in oscillations in pitch attitude, airspeed and other parameters. This is not desirable for many reasons including a decreased performance or discomfort and therefore the use of this autopilot for stabilization at moderate AoA is very limited.

5.2.3 PITCH ATTITUDE CONTROLLER

The last implemented controller sets and holds pitch attitude at a set value and has been described in 5.1.1 as a displacement autopilot. As pictured in FIGURE 39, feedback from the pitch attitude to the elevator stabilizes the closed loop. However, the setting value is somewhat different from the reference and therefore an integration should be added for precise reference tracking.

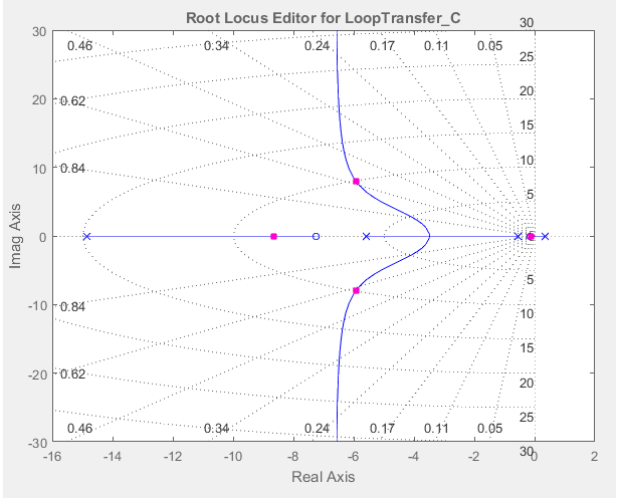

Figure 39: Poles of Closed Loop with Pitch Attitude Feedback

With pitch integration, poles displayed in FIGURE 40 can be stabilized as well. It is notable that the root locus looks similar to the root locus of the pitch rate controller. The only difference between these controllers is the pitch attitude setpoint in the first case and pitch rate setpoint in the second case.

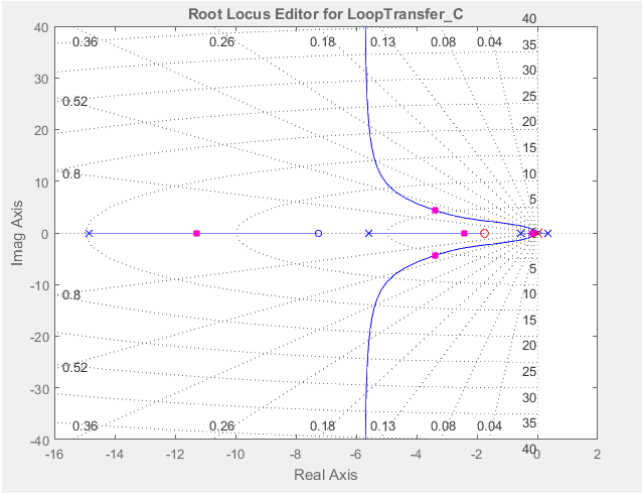

Figure 40: Poles of the Closed Loop with Pitch Attitude PID Controller

To get satisfying performance, PID Tuner tool has been used once again. The constants and performance of the tuned controller can be viewed in TABLE 9.

Controller Parameters

	Tuned
Kp	1.575
Ki	2.2085
Kd	0.16442
Tf	n/a

Performance and Robustness

	Tuned
Rise time	0.134 seconds
Settling time	1.43 seconds
Overshoot	7.24 %
Peak	1.07
Gain margin	-38.1 dB @ 0.337 rad/s
Phase margin	95.7 deg @ 16.5 rad/s
Closed-loop stability	Stable

Table 9: Tuned PID Constants and Performance for Pitch Attitude Hold

The usability of the designed controller for different stability margins of longitudinal motion is investigated in FIGURE 41. The object of interest is the pitch response of different non-linear systems with the same controller. On the left, the required pitch of 10 degrees causes the aircraft to fly at AoA beyond the stall which can be considered an extreme maneuver. A bigger overshoot in case of the unstable configuration is observed. The setting time slightly increases with a CoG location different from the configuration that was used for the PID tuning. Drastic changes in behavior were not observed.

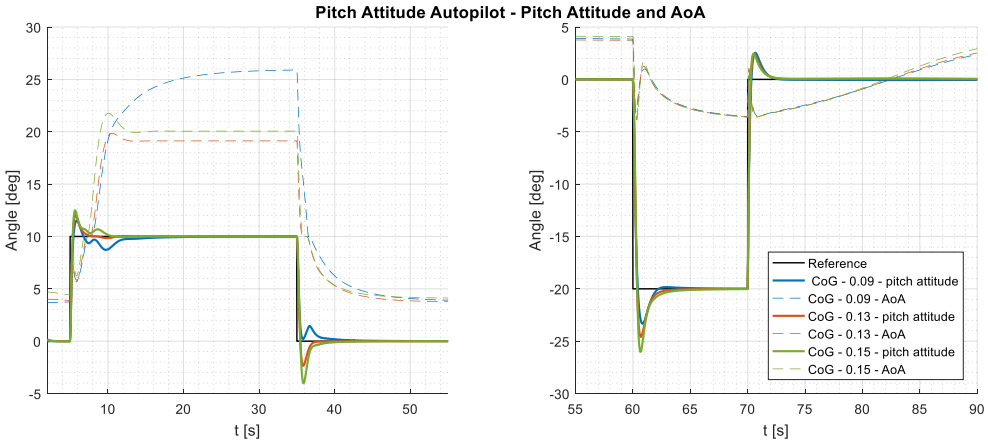

Figure 41: Responses of Designed Pitch Attitude Controller for Different CoG Locations

The control can be improved by switching proportional feedback from pitch attitude directly. [13] Such case produces responses in FIGURE 42 and compared to FIGURE 41, the overshoot is significantly reduced while keeping the setting time similar.

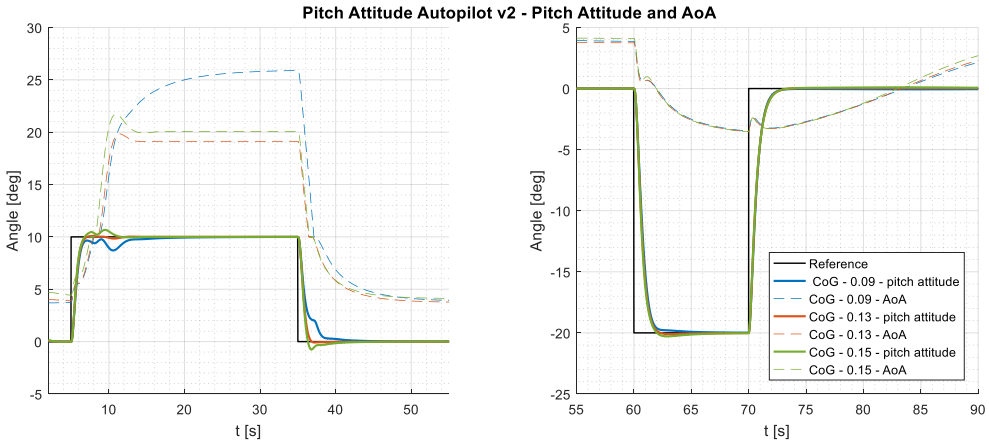

Figure 42: Responses of Designed Pitch Attitude Controller with Direct Pitch Proportional Feedback

5.3 LONGITUDINAL STABILIZATION OF THE TESTBED AIRCRAFT

It is desirable for a glider to fly at the angle of attack that corresponds to the maximum L/D ratio or minimum sink rate respectively. Since the accurate measurement of AoA for small aircraft is complicated (5.1.4), different approach must be chosen. At steady conditions during the flight, a certain pitch angle refers to an approximate of AoA. Therefore, in a moderate wind conditions pitch control can be used to achieve results of reasonable precision.

A proportional controller with a pitch rate damper has been tested. Although the loop was stabilized, this setting provided limited tracking of the reference value with a steady state error. Additionally, the value changed for different configurations because of different trimming demands of an aircraft with different CoG or NP. Therefore, the pitch error integration has been added. Resulting system can be seen in FIGURE 43.

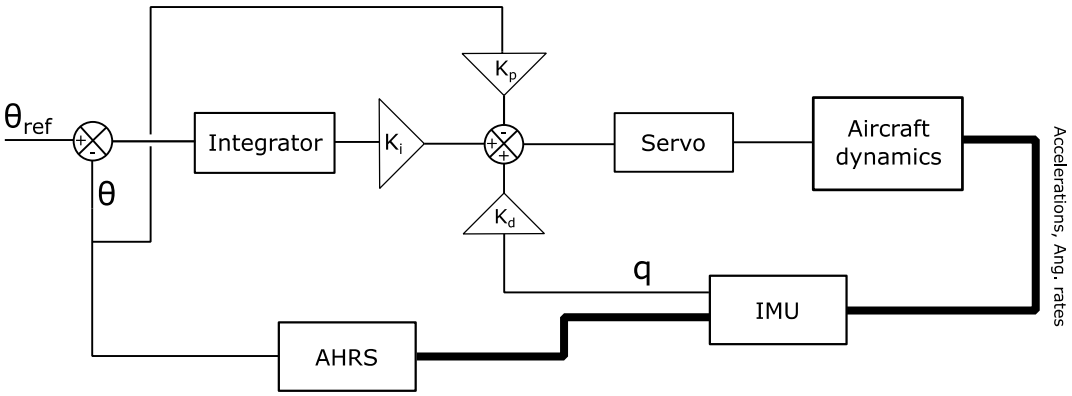

Figure 43: Implemented Pitch Attitude Autopilot

Elevator command is computed with the use of the following equation:

$$elev_{comm}(t) = -K_p \cdot \theta + K_i \cdot (\theta_{comm} - \theta) \cdot \int_0^t d\tau + K_d \cdot Q. \tag{35}$$

For the precise tracking of the reference value, a PID pitch controller has been chosen. Tuning of this controller has been achieved by Ziegler-Nichols method [14], that utilizes heuristic method of tuning the PID controller. In this method, critical proportional gain or ultimate gain $K_{p_{crit}} = K_u$, which keeps the system on the edge of stability, should be experimentally obtained. A system controlled by this proportional gain oscillates with a certain frequency; this frequency is represented by oscillation period T_u.

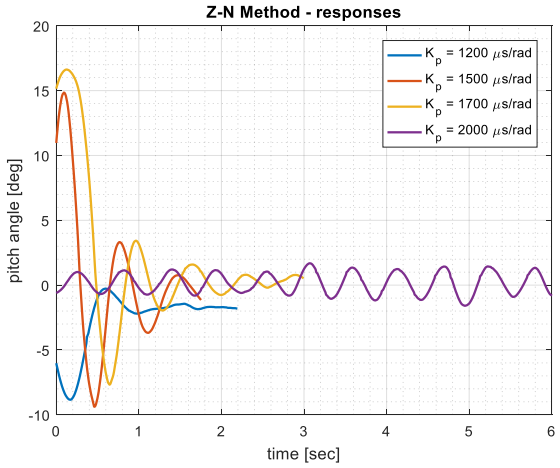

Figure 44: Ziegler-Nichols Method - Pitch Controller Tuning

Ultimate gain and oscillation period were obtained from several in-air tests where the proportional gain was had been risen from numbers verified by the initial P controller as stable to the values

when the loop created consistent oscillations for $K_{p_{crit}} = 2000\ \mu s/rad$ (as shown in FIGURE 44), that were notably undamped from the ground. PID ultimate constants were $K_u = 2000\ \mu s/rad$, $T_u = 0.544\ sec$. Gains for the components of PID are determined using the tuning rule described in [15] as:

$$K_p = 0.2\mathrm{K_u} = 400, \tag{36}$$

$$K_i = \frac{2}{\mathrm{T_u}} K_p = 1471, \tag{37}$$

$$K_d = \frac{\mathrm{T_u}}{3} K_p = 73. \tag{38}$$

Putting (36), (37), (38) into (35), the control law in descrete form is

$$elev_{comm}(k+1) = -400 \cdot \theta(k) + 1471 \cdot \big(\theta_{comm}(k) - \theta(k)\big) \cdot d\tau + 73 \cdot q(k) + elev_{neutral}\,. \tag{39}$$

Final equation for the elevator command is shown above. Sample time $d\tau$ is computed as absolute time difference between steps. Note that $elev_{neutral}$ was added to secure the appropriate length of time-pulses for PWM-controlled elevator servo. The limitations for the elevator command are set to pulse lengths of $1148\mu s$ for the uppermost and $1720\mu s$ for the lowermost deflection of the elevator. These limits match the mechanical and electrical limitations of the whole elevator system. Zero deflection of the elevator is dependent on trim and must not be changed during the test; such action would be reflected in θ_{comm}.

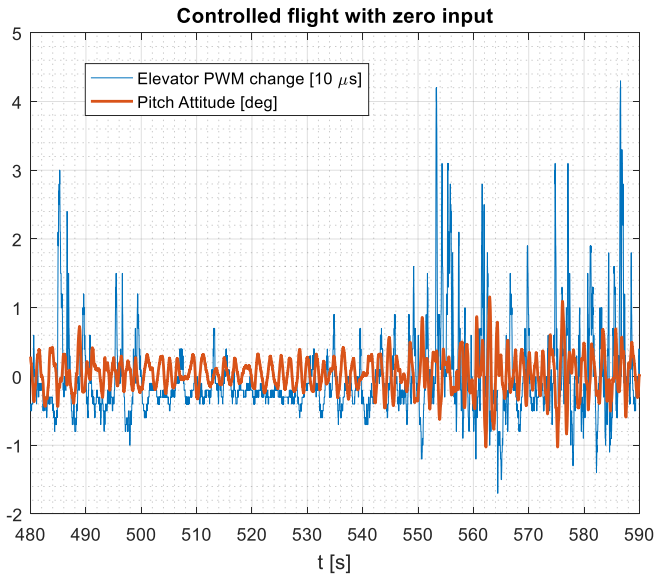

Figure 45: Pitch Attitude Hold - Flight Data

FIGURE 45 shows a flight test of the pitch attitude autopilot with zero input from a human pilot. Pitch attitude as well as control action is shown. Since the stabilized pitch attitude is in the range from -1° to 1°, the controller can be considered sufficient.

The limitation appears to be the speed range, during which this controller takes action in aircraft stabilization. Faster flight, particularly powered climb, makes this controller disproportionately counter the natural pitch up even with a new reference pitch attitude being set. When motor is on, this autopilot is replaced by a low-gain proportional controller, it was examined in earlier stages of controller design. The absence of an airspeed scaler disqualifies this controller from maneuvering tests.

5.4 LATERAL STABILIZATION OF THE TESTBED AIRCRAFT

Similarly to the previous procedure, roll controller was set up utilizing Ziegler-Nichols PID tuning method. The ultimate gain and ultimate period were obtained from several gain-increasing iterations.

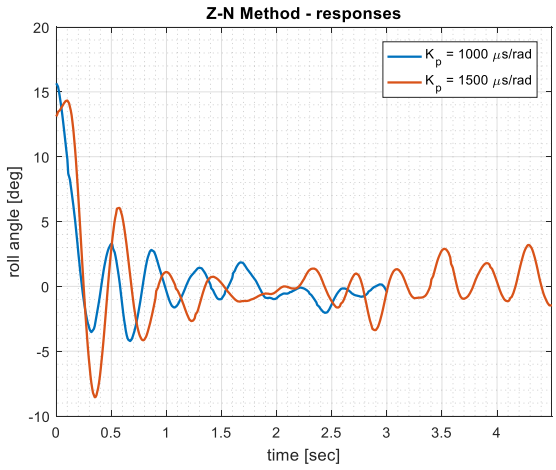

Figure 46: Ziegler-Nichols Method - Roll Controller Tuning

From the flight tests and results in FIGURE 46, ultimate gain was obtained as $K_u = 1500\ \mu s/rad$, ultimate period computed as $T_u = 0.392\ sec$. The PID coefficients corresponding to these values are

$$K_p = 0.2\mathrm{K_u} = 300, \tag{40}$$

$$K_i = \frac{2}{\mathrm{T_u}} K_p = 1531, \tag{41}$$

$$K_d = \frac{\mathrm{T_u}}{3} K_p = 39. \tag{42}$$

The control law to of the roll PID controller is in descrete form defined as

$$\begin{aligned} ail_{comm}(k+1) \\ &= 300 \cdot \left(\phi_{comm}(k) - \phi(k)\right) + 1531 \\ &\cdot \left(\phi_{comm}(k) - \phi(k)\right) \cdot d\tau + 39 \cdot R(k) + ail_{neutral} \\ &\pm ail_{diff} \,. \end{aligned} \tag{43}$$

Here, unlike in case of controlling elevator, besides $ail_{neutral}$, aileron differentiation to improve the rolling ability is added in a form of ail_{diff}. For example, when it is desired to bank right, right aileron goes up with a proportional increase of 50% of initial change of deflection, while the left aileron goes down 50% less than the initial value. That makes the differential proportion of 3:1. This ratio was iteratively set during the initial flights of the testbed aircraft.

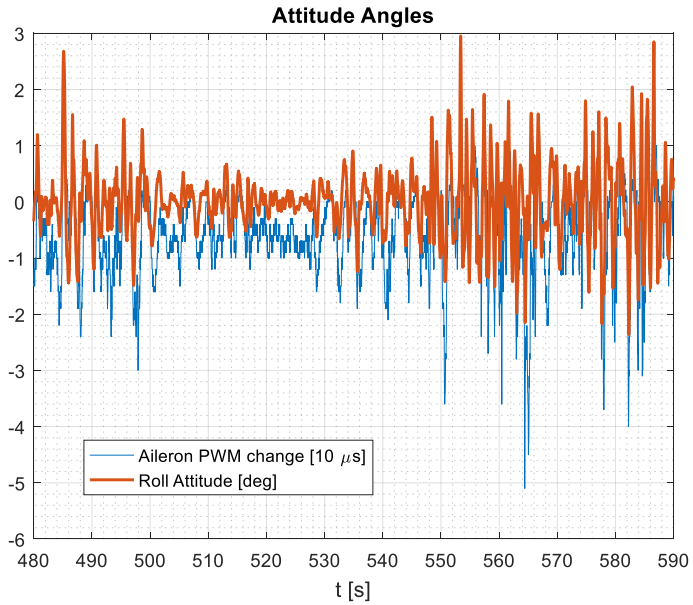

Figure 47: Roll Attitude Hold - Flight Data

Flight test of the tuned roll attitude autopilot with zero input from a human pilot is shown in **FIGURE 47**. Roll attitude as well as control action is shown. The stabilized roll attitude is in the range from -2° to 2°. The deflection from the desired value is greater than in case of the pitch attitude controller. The roll attitude, however, does not affect the flight performance as much as pitch attitude and therefore the roll error is considered insignificant.

In analogy to the pitch attitude autopilot, the limitation of this controller is the absence of an airspeed scaler. In this case, however, a pilot can maintain the desired roll attitude even in case the aircraft is statically unstable in longitudinal motion. A proportional controller with low gain is added to augment the comfort and minimize the pilot input required.

6 SIMULATIONS AND RESULT DISCUSSION

As stated in chapter one, one of the goals of this thesis was the investigation of an aircraft with relaxed stability in terms of performance. During simulations, the model of the testbed aircraft has been used.

6.1 LIFT-TO-DRAG RATIO

First, L/D Ratio is discussed. FIGURE 48 shows an effect of the elevator trim on maximum L/D ratio. This dependency has been chosen to demonstrate the possibility of creating a positive lift on the horizontal tailplane while keeping the drag low enough to increase the performance of the aircraft.

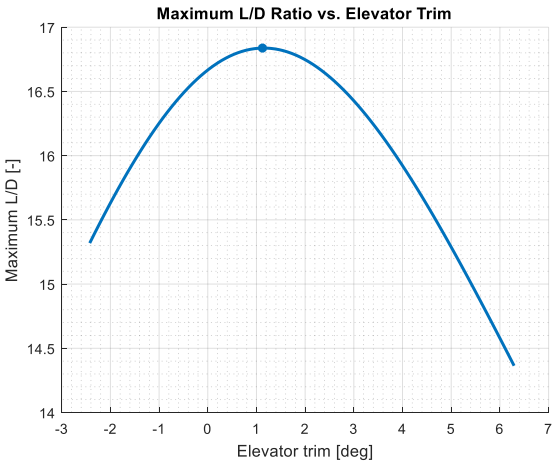

Figure 48: Maximum L/D Ratio vs. Elevator Trim

The maximum L/D ratio along various trims occurs for a small positive elevator trim. Any deflection from this point leads to reduction of the L/D ratio because of the increasing drag caused by the elevator deflection.

6.2 SINK RATE

Similarly to the previous case, an effect of elevator trim is shown in FIGURE 49.

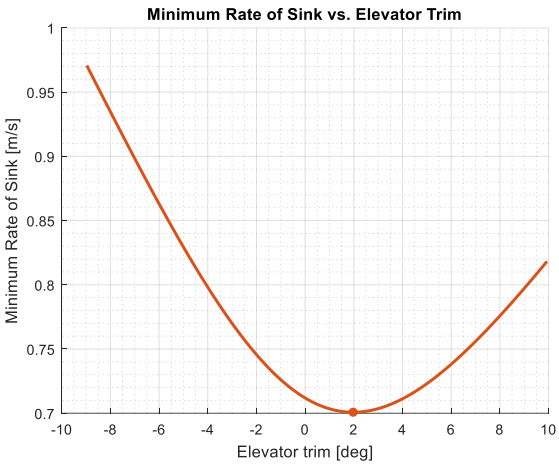

Figure 49: Minimum Sink Rate vs. Elevator Trim

While representing the same simulation model, this figure shows that for the same range of simulated CoG it is required to trim the aircraft with a much greater difference than in case of L/D ratio. This results in greater reduction of performance for the greater elevator deflections. The maximum sink rate performance occurs during a deflection of around 2 degrees, which is slightly higher than for L/D ratio. This contributes to the conclusion that the maximum sink rate tolerates more drag (Section 4.4).

6.3 EFFECT OF VARIOUS AERODYNAMIC CONFIGURATIONS

As the testbed aircraft allows different structure configurations, the simulated influence of these differences on stability and flight performance is discussed in this section.

6.3.1 DIHEDRAL

Dihedral is changeable mainly because of its influence on the lateral characteristics of an aircraft. However, the effect must be investigated to avoid mistakes in longitudinal analysis caused by not taking this parameter into account.

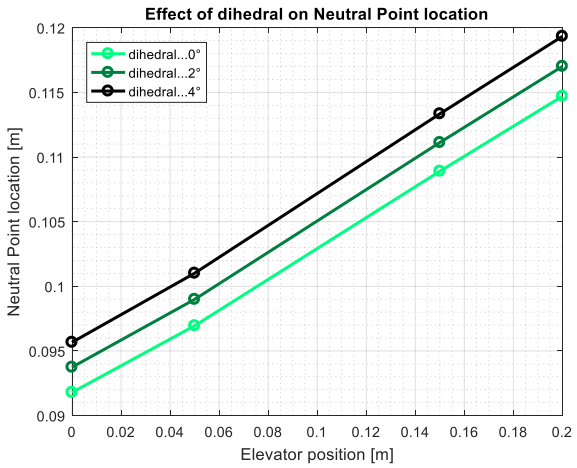

Figure 50: Effect of Dihedral on Neutral Point Location

FIGURE 50 shows an effect of dihedral on neutral point location for different positions of horizontal stabilizer of the aircraft. For greater dihedral, the neutral point shifts backwards with no change to different positions of the horizontal stabilizer and therefore the static stability is increased with an increasing dihedral. This is caused by the higher induced angle of attack towards the wingtips.

6.3.2 HORIZONTAL STABILIZER POSITION

Horizontal stabilizer position is expected to have a strong effect on NP position. Considering the horizontal stabilizer‘s weight, the shift also affects the position of CoG. The position of horizontal stabilizer has a big effect on aircraft’s longitudinal static stability and is investigated in this section closely.

As shown in FIGURE 51, when horizontal tailplane shifted from the most rear position of 0.7 meters from the leading edge of the wing to the position of 0,5 meters from the leading edge, the

longitudinal static stability margin of the aircraft decreases by 0.023m – almost 10% of the mean aerodynamic chord (0.25m).

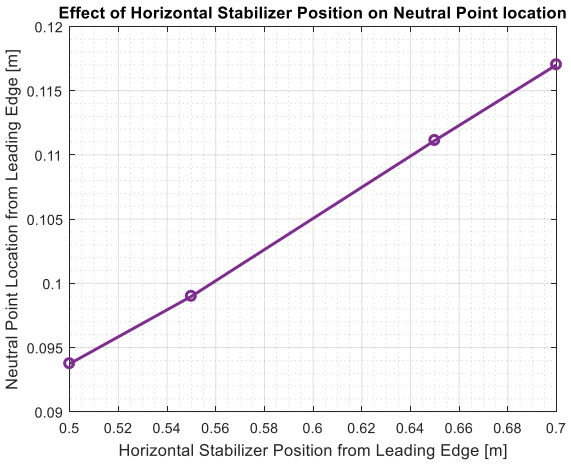

Figure 51: Effect of Horizontal Stabilizer Position on Neutral Point Location

Besides shifting the neutral point, the position change of horizontal stabilizer also affects the angle of incidence for the horizontal stabilizer. Streamlines, passing above and under the wing, are deflected at the wing‘s trailing edge are called downwash. Since the vertical position of the horizontal tailplane is 6,5 cm below the wing level and can be shifted in x-axis only, phenomenon in **FIGURE 52** can be observed.

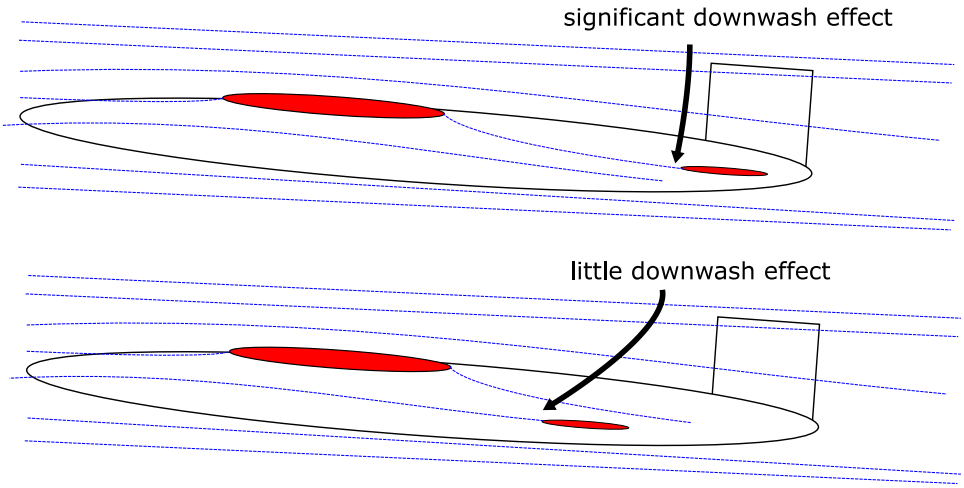

Figure 52: Downwash Effect on Angle of Incidence for Horizontal Stabilizer

As seen in FIGURE 52, for the positions closer to the wing the angle of incidence for horizontal stabilizer is less affected by downwash of the wing. This results in a higher AoA of the horizontal stabilizer which generates more lift or reduces the downward lift of the tail.

Unlike the neutral point differences for different horizontal tail positions with respect to the leading edge of the aircraft displayed in FIGURE 51, L/D ratio maximum that can be seen in FIGURE 53 occurs for close to the same center of gravity. This can be attributed to the effect of downwash angle change described. In case of sink of rate minima, a change of the most viable CoG positions along different horizontal stabilizer positions can be observed. This effect, however, is significantly lowered because of downwash.

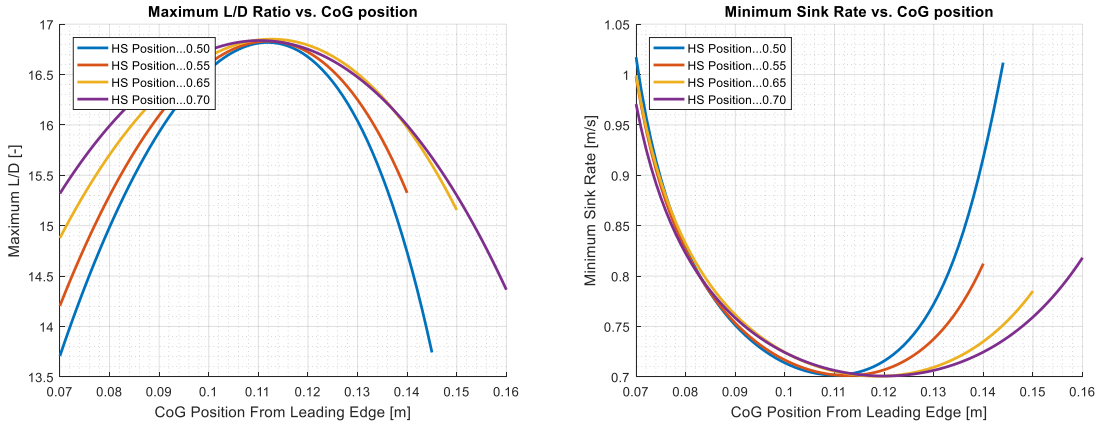

Figure 53: Performance vs. Center of Gravity for Different Horizontal Stabilizer Positions

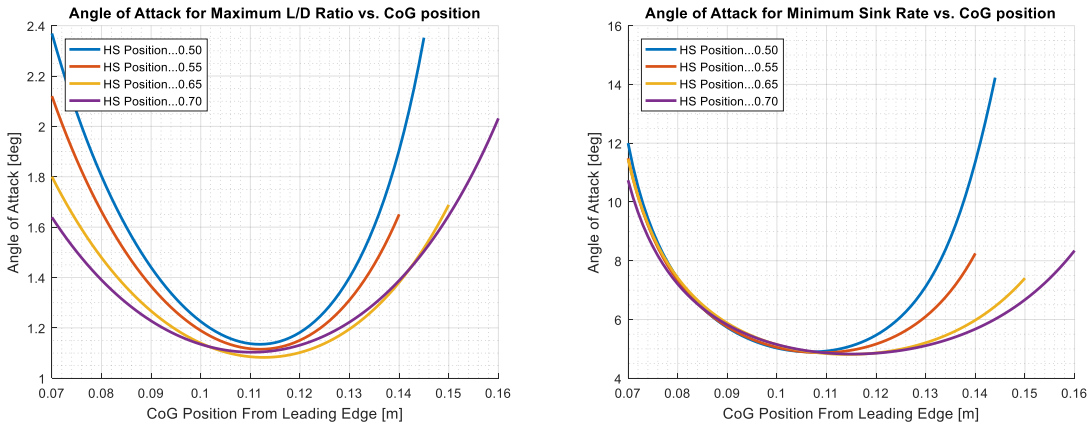

Figure 54: AoA for Max. Performance vs. CoG for Different Horizontal Stabilizer Positions

Angle of Attack aircraft must be trimmed to maximize L/D ratio or minimize sink rate respectively as shown in FIGURE 54. Trimming to the maximum L/D ratio seems to be easier for different CoG location since the difference in values is not high when CoG is changed. On the other hand, when

minimal sink rate is desired, the required AoA rises quickly. Trimming of highly stable or highly unstable configuration is very close to AoA of stall, that is undesired especially in case of unstable aircraft and dangerous state that should be avoided.

Values of AoA for maximum performance along different CoG locations can be seen in **FIGURE 55**. The values are very similar for each horizontal stabilizer position in accordance to the result described in **6.1** and **6.2**. An explanation for this observation might be the fact, that the absolute size of horizontal stabilizer does not change with its position and therefore the lift generated by the horizontal stabilizer combined with elevator deflection stays unaffected as well.

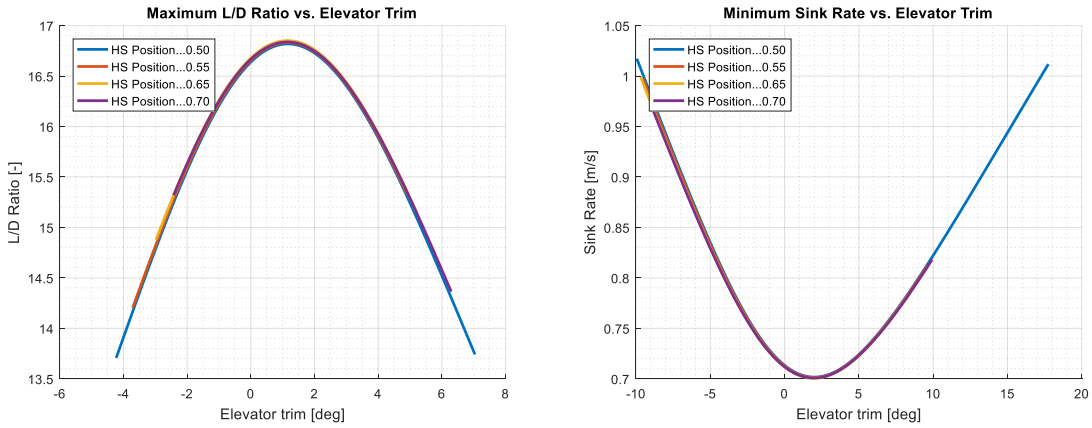

Figure 55: Elevator Trim at maximum Performance - Different Horizontal Stabilizer Positions

However, with a different position of horizontal stabilizer, a wing moment compensation must be increased proportionally to the shortage of the lift force leverage from horizontal stabilizer. When the horizontal stabilizer is shifted towards the wing, its leverage decreases as well as its volume and therefore it is essential to increase the lift by greater elevator deflection, as observed in **FIGURE 56**.

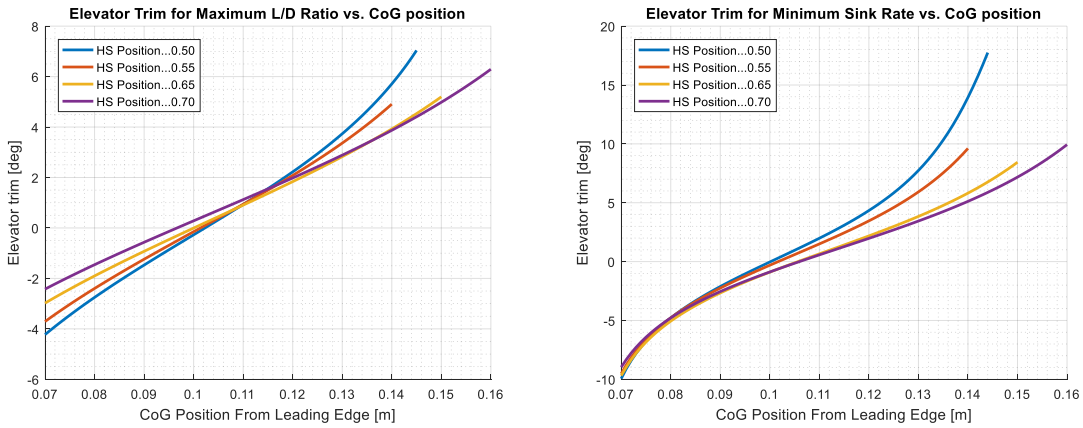

Figure 56:Elevator Deflection for Maximum Performance vs. CoG for Different Horizontal Stabilizer Positions

6.4 DYNAMIC CAPABILITIES

Advantages of dynamic capabilities of an unstable configuration has been investigated widely since aerobatic competitions arose. During aerobatic maneuvers it is desired to keep the track as precise as possible, imprecisions are penalized by lower score. Most of these aircraft, however, do not employ any handling augmentation system and therefore are usually made neutrally stable to minimize the deflections in a straight flight. According to [2], a slow airplane's static instability might improve controllability even without a necessity of computer-aided control system.

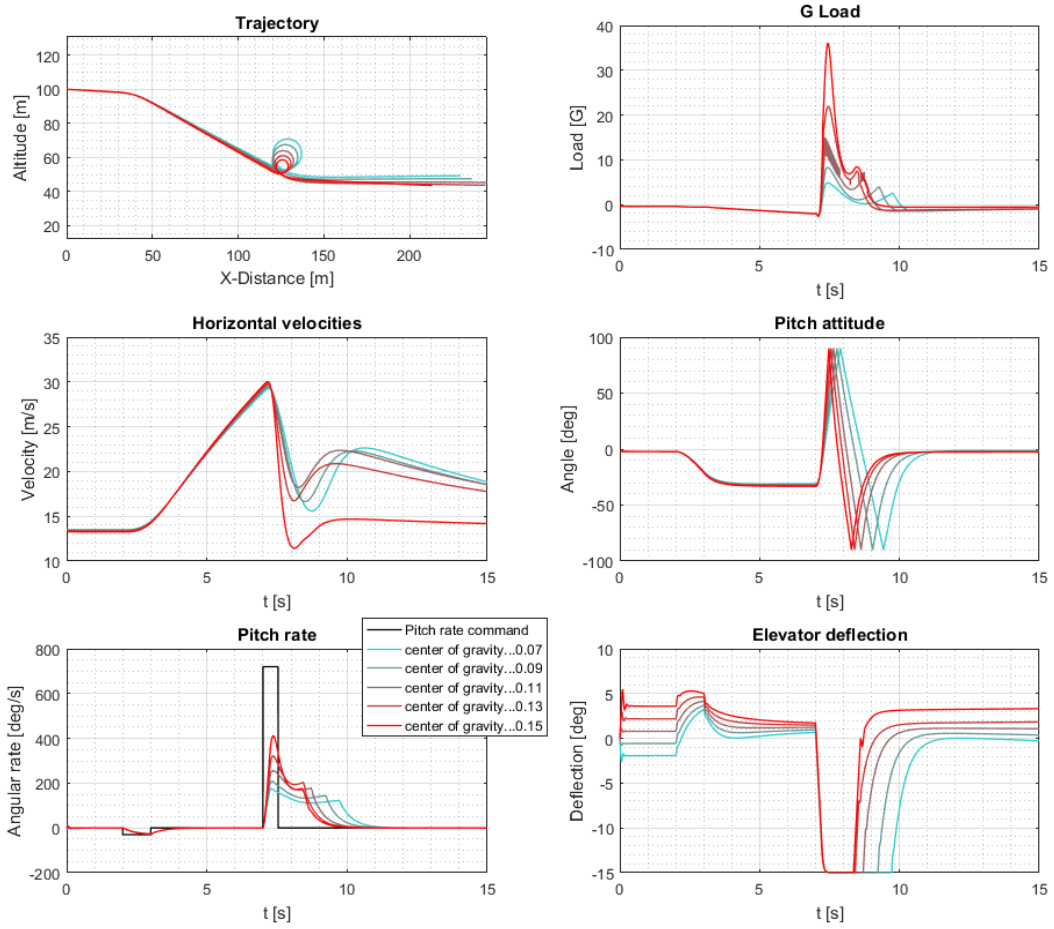

Figure 57: Looping Maneuver of Minimum Possible Radius for Different CoG Position

Static instability helps in maneuvers that require a large change of attitude. Because of the increasing deviation from the trimmed state, aircraft tends to complete the maneuver itself after an initial 'kick' without any further control. For jet fighters, the maneuverability is supported with a static longitudinal instability as well as other augmentation systems like thrust vectoring. Using

these systems establish an ability to perform maneuvers impossible using just aerodynamic mechanisms (supermaneuverability) [16].

FIGURE 57 shows a simulated looping maneuver performed by the testbed aircraft. In this simulation, the elevator deflection is limited to ± 15 degrees and the aircraft is made to complete a looping maneuver of minimal radius and maximal possible pitch rate. Is is shown that for the same elevator deflection the rearest possible CoG position enables aircraft to pitch much faster than during the previous cases. The limitation might be the structural endurance that must withstand a high load reaching up to 40G. Load factor in case of the most stable simulated configuration is much lower, around 5G.

6.5 VISUALIZATION IN FLIGHTGEAR

To observe and verify the aircraft behavior during all tests, a link between MATLAB's Simulink and FlightGear flight simulator has been established. This has been achieved by sending Simulink model's telemetry packets via UDP. A custom head-up display (HUD) has been created to visualize the AoA and pitch angle.

After transformations, the following quantities are sent in the before mentioned UDP packet:

- Position
  - Latitude
  - Longitude
  - Altitude
- Attitude angles – yaw is arbitrarily set to fit the scenery, roll is zero
- Angle of Attack – for HUD display
- Airspeed
  - Calibrated Airspeed
  - Velocity with respect to each axis
- Elevator deflection
- Motor thrust converted to RPM

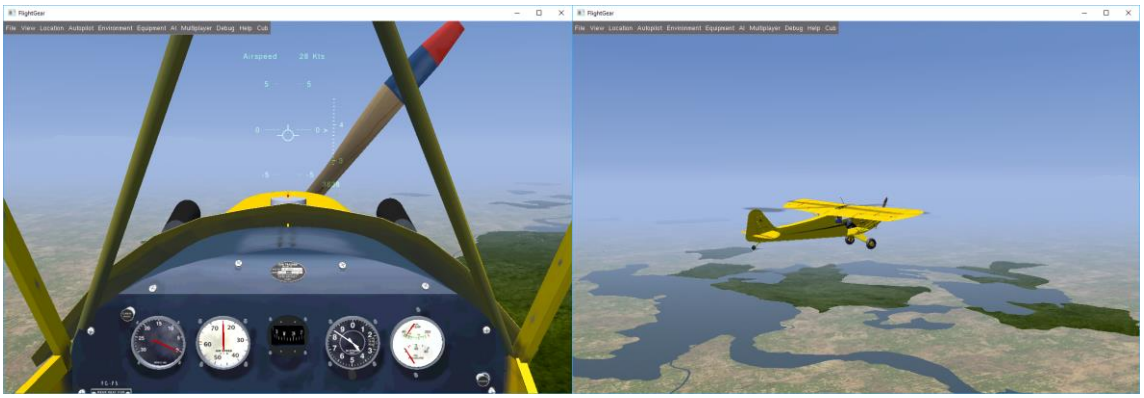

Figure 58: FlightGear visualization

Elevator deflection has been multiplied by a constant to emphasize a small elevator deflection. This way, every aspect of the flight characteristics is visualized in FlightGear engine and can be easily observed. The flight simulator's engine is not only used to visualize the pre-set simulations, but also as a visualization of simulations with human controlling the thrust and elevator deflection using joystick or keyboard. The result is displayed in FIGURE 58.

7 FIELD TESTS AND RESULT DISCUSSION

Field tests are an important part of simulation results verification. In this chapter, field tests are designed beforehand and carried out at a suitable location. Finally, the field tests results are discussed and compared to simulations in the end of this chapter.

7.1 FIELD TESTS SCENARIOS

Before the flight tests, flight scenarios must be designed and verified. These scenarios should have a form of parts of the flight designed in such way to get the most precise results possible while minimizing the effort and potential errors.

Parameter	Value
Horizontal stabilizer position	0.7 m
Vertical stabilizer position	0.7 m
Dihedral	2 deg

Table 10: Testbed Aircraft's Configuration for Field Tests According to Figure 13

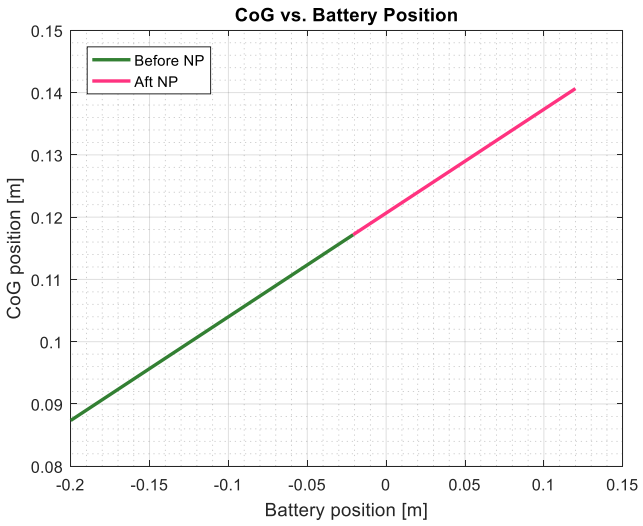

Figure 59: CoG Position during Battery Position Modification for the Tested Configuration (Table 10)

To simplify the flight tests, structure parameters were fixed during the flight experiments. The chosen configuration (as shown in TABLE 10) had the dihedral set to 2° and the position of

horizontal and vertical stabilizers was set to 0.7 m. The possible movement of battery enabled the CoG to be shifted as shown in FIGURE 59.

7.1.1 GLIDE PERFORMANCE SCENARIO

It is desired to set up the appropriate pitch for the attitude controller described in 5.3. To prevent unwanted deflections by setting different pitch attitude for different CoG locations, it was decided to set one pitch attitude reference for all tested CoG positions. This approach was verified by simulations.

In FIGURE 60, the simulated performance of the testbed aircraft with a pitch attitude reference set to 0 degrees is shown. Compared to the simulations in Chapter 6 similar curve shapes could be observed. Degradation of the results occurs only for CoG positions further from the best gliding performance locations. However, the predicted trend could be proven with this approach.

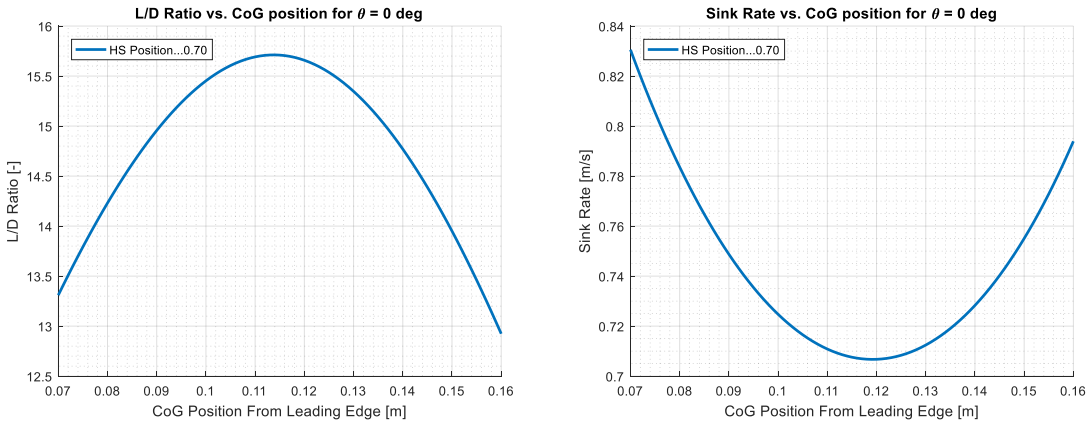

Figure 60: Simulated Performance of the Gliding Testbed Aircraft at Pitch Attitude set to 0 degrees

As the trend is preserved, it is necessary to verify the airworthiness of the aircraft with the controller set to mentioned value. To do this, simulation of AoA and elevator trim was performed prior to flight tests. Result of the simulation is shown in FIGURE 61. Having an AoA in the approximate range of 3.5 to 4.5 degrees does not reach a critical AoA for a high risk of unwanted wing stall. The elevator trim must be checked with caution especially in the unstable range of CoG. A sufficient safety margin of further positive elevator deflection should be implemented. In the case of the maximum elevator trim of 8 degrees, the margin is sufficient to maintain control over the aircraft in case of unexpected situation.

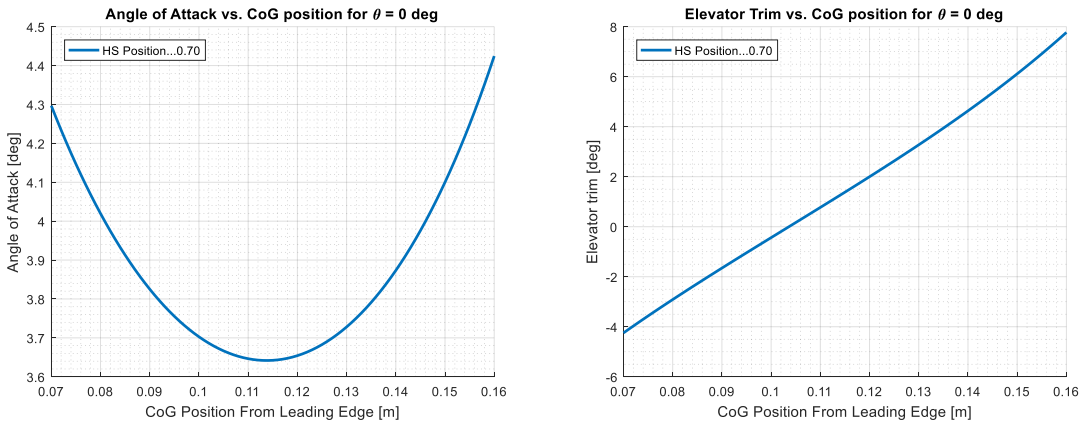

Figure 61: Simulated AoA and Elevator Deflection for the gliding Testbed Aircraft at Pitch Attitude set to 0 degrees

Glide performance is ideally investigated during a straight flight of constant speed, sink rate, L/D ratio and attitude angles. This is difficult to achieve with a small glider. Roll and pitch attitude angle are stabilized by control system proposed and described in **5.3** and **5.4**. However, these systems cannot stabilize the flight path and in this case, it is not a big limitation to "let the aircraft fly its own path". This way, the control action is minimized and therefore the error should be minimal. To select such parts of the flight, inputs from the pilot described in **3.4.2** are monitored and situations when the pilot controls the aircraft are not considered. This results in a flight at constant roll and pitch attitude while keeping close to straight flight path.

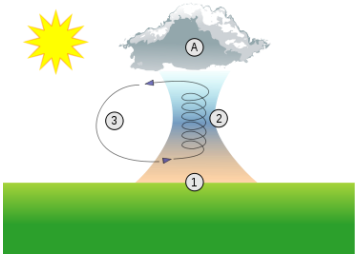

Figure 62: Thermal Column[3]

Another limitation is the thermal phenomenon in the air during the day. As solar radiation heats up ground unevenly, the air directly above the ground is being heated unevenly as well. This creates thermal columns as can be seen in **FIGURE 62** and read about in [17]. Thermals are used by gliders and soaring birds to gain altitude. The air flow is being compensated by downward streams. In this scenario, however, thermals cause error that cannot be compensated. To minimalize the thermals,

[3] By Dake - Self-made illustration, CC BY 2.5, https://commons.wikimedia.org/w/index.php?curid=1336974

flight tests took place in the morning, when the ground was not heat up yet and therefore the thermal occurrence was limited. In the morning, the wind was also often minimal considering the whole day.

7.1.2 MANEUVERABILITY SCENARIO

To test and verify the simulation results of the dynamic behavior of the aircraft (Section 6.4), the scenario must be designed carefully with respect to the structure of the testbed aircraft. Since the main lifting components – wing and horizontal stabilizer – are connected by rubber bands, the connection is rather movable and cannot be considered solid, strong, and stable during maneuvers with high load. During initial flight tests focused on PID tuning it was observed that the tailplane is the critical part of the structure and its mount can withstand only a very limited range of load, because the negative lift of the horizontal stabilizer was stronger than the rubber bands causing flatter and dynamic instability in higher speeds.

The maneuverability observation takes place under set pitch rate while the real response and forced elevator deflection are observed. This way, differences among various locations of CoG can be seen by comparing these parameters.

7.2 FIELD TEST RESULTS

Parts of the flight suitable for analysis are carefully chosen from the flight log. The most basic criteria in glide performance testing feature:

1. Disabled motor,
2. Enabled stabilization,
3. No thermal influence,
4. No pilot input,
5. Acceptable pitch and roll attitude.

These can be verified from postprocessed flight data. To make the analysis convenient, an output similar that shows motor input, autopilot switch input, attitude, and altitude is studied (as shown in FIGURE 63). First two properties can be determined by observing the motor input being zero and autopilot switch being above zero.

The altitude changes give a hint of whether the measurement is affected by a thermal. The change of altitude in FIGURE 63 is smooth and represents a flight unaffected by a thermal. Different

situation is pictured in FIGURE 64, where the altitude shows rapid changes in descent. These are caused by thermal columns. Noteworthy part of the flight starts right after the motor is shut down. The altitude drop is a consequence of the aircraft getting the cruising speed at the pitch attitude set by the controller. For the performance analysis, only the part after the change of altitude for the airspeed should be considered.

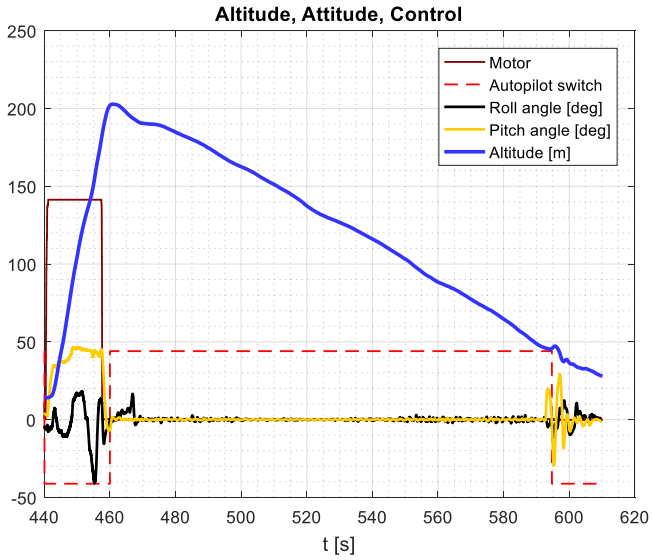

Figure 63: Flight Telemetry and Scaled Control Data

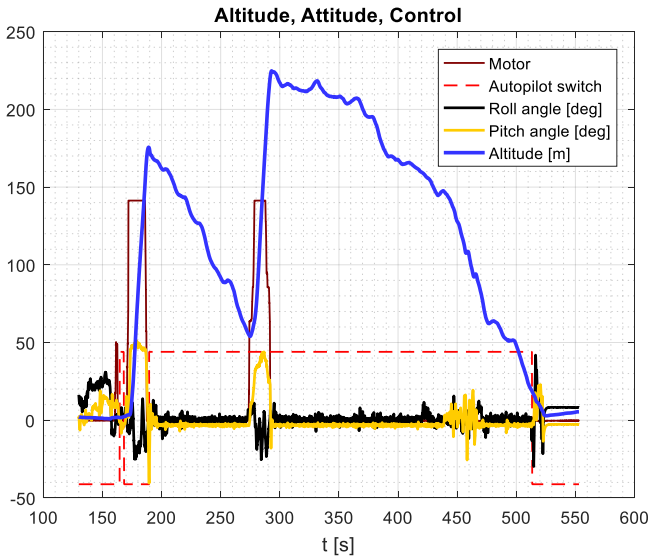

Figure 64: Altitude affected by a Thermal

The last two criteria of no pilot input and acceptable attitude angles are derived directly from corresponding logs. As shown in FIGURE 65, the reference attitude angles are maintained with just

small deviations and the pilot input is zero approximately from 470 to 590 seconds. Considering FIGURE 63, the part for further investigation would be the the steady flight from 480 to 580 seconds.

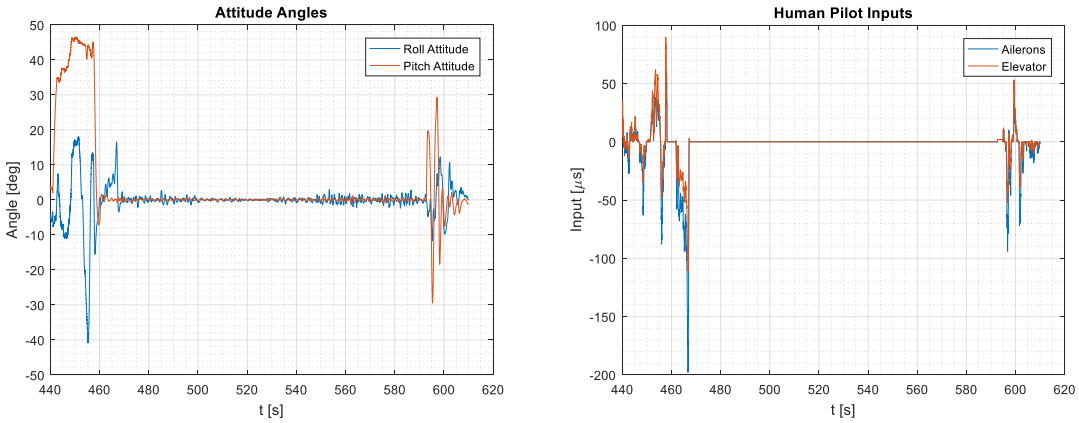

Figure 65: Attitude Angles and Human-Pilot Input

As can be seen in FIGURE 66, the trajectory of the flight is not straight. Because of the asymmetricity, the aircraft tends to fly in circles of a big radius. This contributes to the precision of the results when wind is present. The wind affects the trajectory by an almost constant shift in time. The previously determined part of the flight is shown as well to verify the smoothnes of the flight path and discover a potential change of the wind.

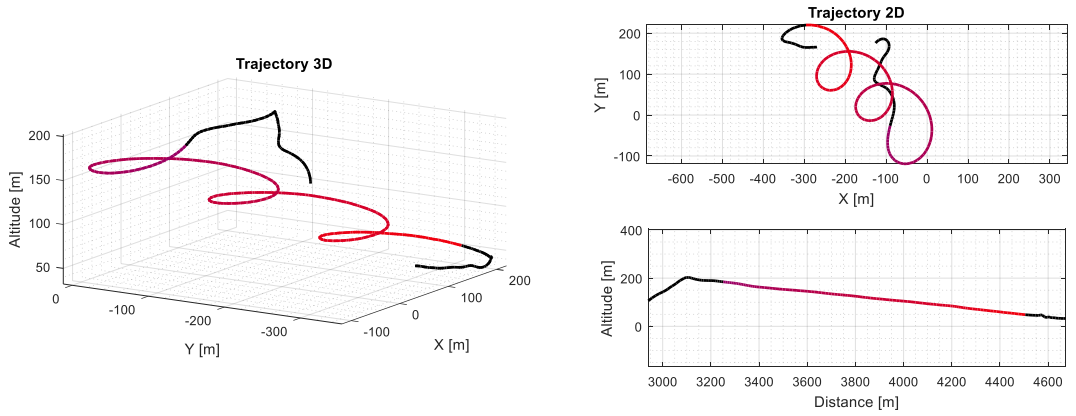

Figure 66: Flight Path - 3D and 2D

The influence of wind can be eliminated only if the complete circle is flown. Since the precise heading was not available during the tests, a flight path to close the full circle was determined manually. The result can be seen in **FIGURE 67**.

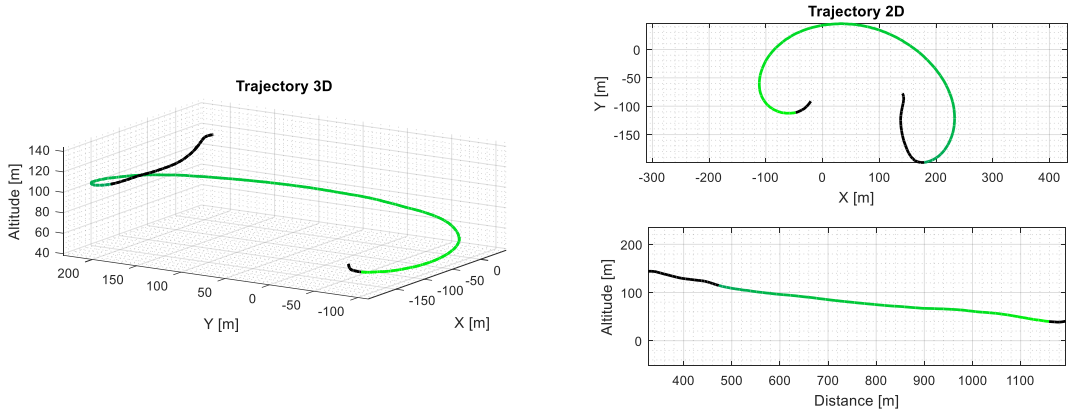

Figure 67: Part of the Flight Considered for Analysis

To get reasonable accuracy, the previous procedure was repeated from two to four times for every tested configuration. The flight tests have been performed during several sessions and since the results varied from day to day, they are grouped by the session.

θ_{ref} = 0 deg			
battery position	-0.2000	-0.165	-0.13
sink rate	1.2595	1.0877	1.1016
glide ratio	9.4856	9.9973	11.4518

Table 11: Flight Performance of Stable Configuration at θ_{ref} = 0 deg

TABLE 11 shows the performance for stable configurations at reference pitch attitude being zero. Flying at high AoA and vicinity of stall was notable while the aircraft was being controlled. To prevent unexpected risky situations, the reference pitch attitude was set to -3 degrees.

θ_{ref} = -3 deg			
battery position	-0.2000	-0.165	-0.13
sink rate	1.5844	1.4505	1.3978
glide ratio	9.1454	9.8421	10.7191

Table 12: Flight Performance of Stable Configuration at θ_{ref} = -3 deg

At this attitude, the testbed aircraft's performance decreased as shown in TABLE 12. The differences are, however, preserved, whichconfirmed the usability of this resolution.

θ_{ref} = -3 deg			
Battery position	-0.1300	0	0,05
Sink rate	1.3534	1.2706	1.3396
L/D ratio	10.5466	10.7095	10.3795

Table 13: Flight Performance of Stable Configuration at θ_{ref} = -3 deg

The results for stable as well as unstable configurations are shown in TABLE 13. The highest performance of the three tested configurations is observed for battery position right under the leading edge of the wing. According to the simulation, this location causes CoG moving aft the NP. The flight test confirmed dealing with unstable configuration. In FIGURE 68, the control action of the stabilization can be seen from 250 seconds. At 252.5 seconds, the aircraft stabilization was disabled. The aircraft immediately started to pitch up, which was countered with the elevator. The correction did not put the aircraft in steady flight and therefore the control system had to be employed again.

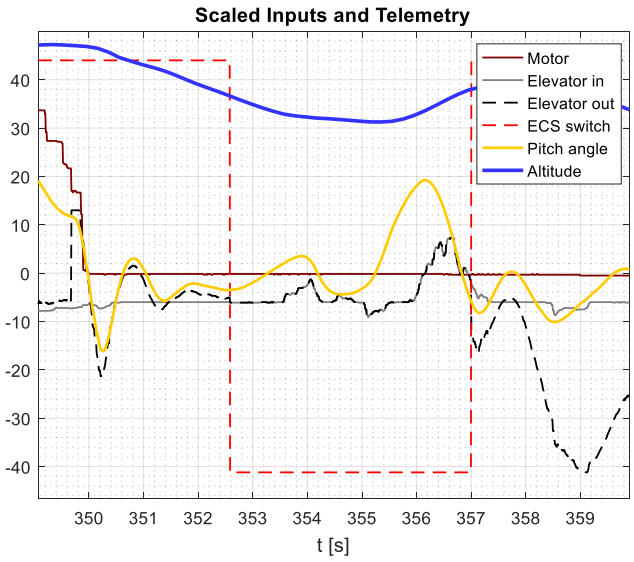

Figure 68: Stability Test – Configuration With Battery Placed at 0m

Averaged results are shown in FIGURE 69. As determined from the simulations, the trend can be approximated by a second-degree polynomial. Different battery positions affect the flight performance significantly. The optimal sink rate occurs for battery position slightly aft the position for optimal L/D ratio. By shifting the battery from -0.2 to 0.0m, a relative improvement of 17% in range and 20% in endurance could be achieved.

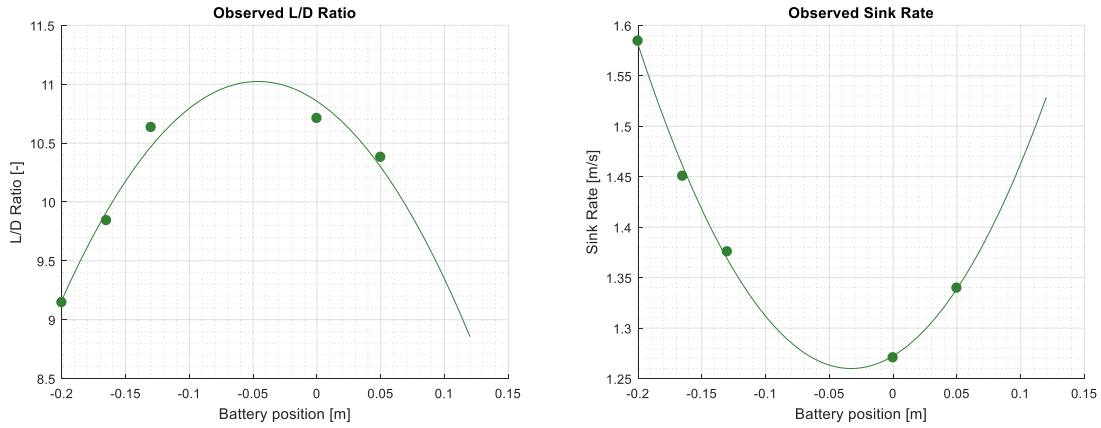

Figure 69: Observed performance indicators

7.3 COMPARISON WITH SIMULATION

The performance of the testbed aircraft is much lower than expected, based on the simulation results. FIGURE 70 shows that the different battery positions affect both the L/D ratio and the sink rate in a more significant way than during the corresponding simulation experimens. This increased sensitivity to battery position may correlate with the NP lying more in the front than simulated NP for the tested position of the horizontal stabilizer (as discussed in section 6.3.2). This statement is supported by the fact that in simulations, the battery position of 0.0 m with respect to the leading edge of the wing represented a marginally unstable configuration (pictured in FIGURE 59), while during the performed flight tests the stability seemed to be vastly negative. A possible cause of this observed differenece might be the limited aerodynamic simulation of the fuselage, which might have created a significant lift that might have changed the pitching moment and shifted the NP location forwards. Zero elevator deflection trim for the configuration with the frontest battery position during a flight without the stabilization setting supports this conclusion.

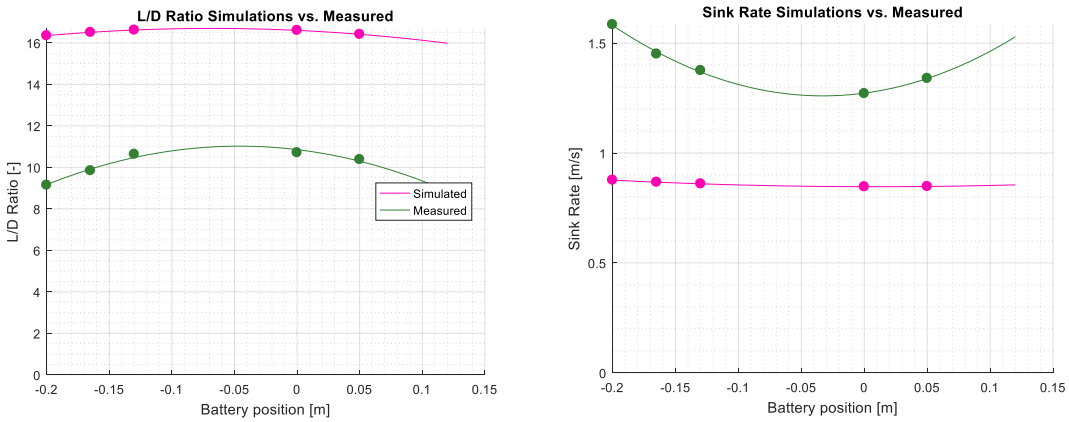

Figure 70: Simulation vs. Measurement Performance Comparison

The decreased performance is caused by a combination of several factors:

- Parasitic static drag from additional parts of the aircraft that were not simulated
  - Rubber bands for mount of horizontal stabilizer and vertical fin and the wing to the fuselage,
  - Fold propeller,
  - Servo mounts and servo cables at the aircraft's tail,
  - Non-perfect smoothness of the covering material (mainly due to pollen stuck to the surfaces),
- Mechanical factors:
  - Performance of the flight tests in non-steady conditions that required frequent action of the controller,
  - Neglecting the lateral motion during the simulation experiments,which could play a big role in decreasing the performance because of the sideslip angle as well as the control action on ailerons creating an additional drag.

A combination of these could represent the reasons for the differences observed during the result comparison.

8 SUMMARY AND CONCLUSIONS

The aim of this study was to investigate relaxed longitudinal static stability and its effect on the flight performance. Goals of this thesis were formulated as follows:

1. Simulate glider performance on a mathematical model with preliminary accuracy
2. Verify the simulation results by performing flight tests on configurable testbed aircraft
3. Assess the effect of relaxed static stability on flight performance

To achieve these goals, a testbed aircraft was designed. Configurability was implemented by a possibility of shifting the tailplane, changing dihedral and providing a variety of center of gravity locations by moving the battery. A mathematical model of longitudinal motion was developed and supported with data from aerodynamic analysis of the testbed aircraft. Flight control systems that stabilize an unstable configuration were described and applied during the simulation. The linear simplification of the mathematical model was analyzed and used for tuning of the flight control systems. The effects of various configurations on static stability and aircraft performance were simulated in MATLAB Simulink. A pitch attitude autopilot was determined as the most suitable setting for a glider. It was observed that for higher dihedral the neutral point is shifted slightly backwards because of the increased induced angle of attack. Substantial effect of the horizontal stabilizer position on neutral point location was confirmed. Although the maximum performance was not affected by location of horizontal stabilizer, higher sensitivity to a center of gravity change was observed for horizontal tailplane closer to the wing.

Flight scenarios were designed to verify the simulations and quantify the real performance of the testbed aircraft. The values obtained showed bigger differences across various locations of center of gravity than simulations, corresponding to the simulation results of an aircraft with neutral point located more to the front. The differences were caused by the simplifications in the aircraft's aerodynamic analysis for the mathematical model. However, flight tests have shown the possibility of improvement in gliding performance with relaxed static stability.

There were several limitations during the tests. Among the biggest limitations, the reliability of the designed control system hardware could be mentioned. Since the computational unit operates linux, it is prone to failures. Although experienced only once during the flight tests resulting in an uncontrolled crash, these failures represent a potential hazard for the surrounding area including people. This limitation could be eliminated by designing a forward embedded system that would secure the handling in case of the main system failure. Another limitation experienced during the flight tests were high requirements for the flatness and obstacle-free spacious ground. Influence of

the ground slope was reduced by a careful choice of the experimental spot, but could not be eliminated entirely. Despite these limitations, the results fulfilled the initial goal of this thesis.

This master's thesis presented an approach utilizing flight tests to verify simulations. Further investigation of different configurations and their impact on the flight performance poses an interesting challenge. Future effort could result in aircraft structure and configuration recommendations to get the best possible gliding characteristics. The flight data acquired could be also used for a development of more sophisticated control systems.

BIBLIOGRAPHY

[1] "CG Location by Dr. Mark Drela," [Online]. Available: http://www.charlesriverrc.org/articles/supergee/CGMarkDrela.htm. [Accessed 1 May 2018].

[2] P. Kämpf, " Are fighter jets designed to be so inherently unstable that a human can't fly one unassisted?," 13 April 2017. [Online forum comment]. Available: https://aviation.stackexchange.com/a/8061. [Accessed 7 May 2018].

[3] En.wikipedia.org, "Gliding flight," [Online]. Available: https://en.wikipedia.org/wiki/Gliding_flight. [Accessed 17 March 2018].

[4] N. Hall, "Center of Pressure - cp," 5 May 2015. [Online]. Available: https://www.grc.nasa.gov/www/k-12/airplane/cp.html. [Accessed 14 5 2018].

[5] S. O. Madgwick, "An efficient orientation filter for inertial and inertial/magnetic sensor arrays," University of Bristol, Bristol, UK, 2010.

[6] T. I. Fossen, "Mathematical Models for Control of Aircraft and Satellites, 2nd edition," Norwegian University of Science and Technology, Trondheim, NO, 2011.

[7] Desktop Aeronautics, Inc., "Applied Aerodynamics: A Digital Textbook," Desktop Aeronautics, Inc., Stanford, US-CA, 2007.

[8] M. Peters and M. A. Konyak, "The Engineering Analysis and Design of the Aircraft Dynamics Model For the FAA Target Generation Facility," Federal Aviation Administration, Atlantic City, US-NJ, 2012.

[9] J. H. Blakelock, Automatic Control of Aircraft and Missiles Second Edition, New York: John Wiley & Sons, Inc., 1991.

[10] A. S. Rueda, "Design and Testing of a Flight Control System for Unstable Subscale Aircraft," Master's thesis, University of Linköping, Linköping, SE, 2015.

[11] J. E. Zeis, "Angle of Attack and Sideslip Estimation using an Inertial Reference Platform," Master of Science, Air Force Institute of Technology, Ohio, 1988.

[12] F. A. P. Lie, "Synthetic Air Data Estimation," Dissertation, University of Minnesota, US-MN, 2014.

[13] M. Hromčík, *Flight Control Systems course*, Prague, Spring Semester 2016/2017. Available: https://moodle.fel.cvut.cz/course/view.php?id=1712.

[14] J. G. Ziegler and Nichols, N. B., "Optimum settings for automatic controllers," Rochester, US-NY 1942. [Online]. Available: https://staff.guilan.ac.ir/staff/users/chaibakhsh/fckeditor_repo/file/documents/Optimum Settings for Automatic Controllers (Ziegler and Nichols, 1942).pdf.

[15] Microstar Laboratories, "Ziegler-Nichols Tuning Rules for PID," 2018. [Online]. Available: http://www.mstarlabs.com/control/znrule.html. [Accessed 22 March 2018].

[16] En.wikipedia.org, "Supermaneuverability," 2018. [Online]. Available: https://en.wikipedia.org/wiki/Supermaneuverability. [Accessed 7 May 2018].

[17] En.wikipedia.org, "Thermal," [Online]. Available: https://en.wikipedia.org/wiki/Thermal. [Accessed 2 May 2018].

APPENDIX A: CONTENT OF THE ENCLOSED CD

The attached CD contains resources required to replicate the results of this thesis at full scale:

- Directory '**Construction'** contains drawings of the wing and the tailplane,
- Directory '**FlightGear'** contains hud file for a flightgear model and .bat launch file,
- Directory '**MATLAB'** contains Simulink models and codes for data processing,
- Directory '**Onboard_codes'** contains codes and custom software used for the testbed aircraft,
- Directory '**real_data'** contains data from test flights relevant to results section of this thesis.
- File '**DP_kubica.docx'** is MS Word 2016 source file,
- File '**DP_kubica.pdf'** is electronic version of this thesis.